RHEOLOGICAL INVESTIGATION OF COLLOIDAL SYSTEMS

by
OMID AKHLAGHI BAGHOOJARI

Submitted to the Graduate School of Engineering and Natural Sciences
in partial fulfillment of
the requirements for the degree of
Doctor of Philosophy

Sabanci University
August 2017

RHEOLOGICAL INVESTIGATION OF COLLOIDAL SYSTEMS

APPROVED BY:

Asst. Prof. Dr. Ozge Akbulut.....
(Thesis Supervisor)

Asst. Prof. Dr. Fevzi Çakmak Cebeci.....

Asst. Prof. Dr. Meltem Elitas.....

Prof. Dr. Nergis Arsu.....

Prof. Dr. Metin Acar.....

Assoc. Dr. GÖZDE İNCE

DATE OF APPROVAL: 01/08/2017

ABSTRACT

RHEOLOGICAL INVESTIGATION OF COLLOIDAL SYSTEMS

Omid Akhlaghi Baghoojari

PhD Dissertation, August 2017

Supervisor: Assist. Prof. Ozge Akbulut

Keywords: Suspension, graft-copolymer, rheology, stability

Ceramic processing such as cementation and casting are among the most widely used methods for production of commercial products with different size and properties to date. Highly loaded and stable aqueous suspensions whose rheological behavior can be controlled by low content of organic additives are highly desired. To have control over the viscosity and improve fluidity/solid loading of ceramic suspensions, different series of polycarboxylate ether-based copolymers (PCEs) that include acrylic acid, 2-acrylamido-2-methylpropane sulfonic acid, vinylphosphonic acid, and polyethylene glycol-1000 were synthesized. The effect of monomer feed ratio and molecular weight of copolymer on dispersing ability of the copolymers, fluidity of the pastes, and rheological behavior of suspensions were characterized and performance of these copolymers as rheology modifiers was reported. For the first time in literature, dedicated superplasticizers for i) calcium aluminate cement (CAC) and ii) ordinary portland cement-calcined clay-calcium carbonate ternary blends were synthesized such that they caters to the characteristic properties of these systems; i) high rate of surface development and surface charge in CAC and ii) layered structure of calcined clay and high concentration of sulfate ions in ternary blended

cement. The effect of PCEs on i) rheological behavior of alumina suspensions and ii) fabrication of highly loaded alumina suspensions and machining of solid cast green bodies were also investigated. While 20 vol. % pure alumina suspensions showed severe particle jamming, 35 vol. % alumina suspensions with more than 1 wt. % copolymers displayed Newtonian behavior. These suspensions found to be suitable for fabrication of solid cast green bodies and provided ability of significant removal of material in machining process.

OZET

RHEOLOGICAL INVESTIGATION OF COLLOIDAL SYSTEMS

Omid Akhlaghi Baghoojari

PhD Dissertation, August 2017

Supervisor: Assist. Prof. Ozge Akbulut

Keywords: Süspansiyon, asılı kopolimer, reoloji, stabilite

Çimentolama ve döküm gibi seramik işlemleri, günümüze kadar farklı boyut ve özellikteki ticari ürünlerin üretimi için sıklıkla kullanılan yöntemler arasında olmuştur. Reolojik davranışları, düşük miktarda organik katkı maddeleri ile kontrol edilebilen yüksek miktarda yüklü ve kararlı sulu süspansiyonlar çokça tercih edilmektedir. Akrilik asit, -akrilamido-2-metilpropan sülfonik asit, vinilfosfonik asit ve polietilen glikol-1000'i içeren farklı seri polikarboksilat eter bazlı kopolimerler (PCE'ler) viskoziteyi kontrol altına almak ve seramik süspansiyonların akışkanlığını/katı yüklenmesini iyileştirmek için sentezlenmiştir. Kopolimerlerin dağılabilme yeteneği, macunların akışkanlığı ve süspansiyonların kayma ve genleşmeli reolojik davranışları üzerine kopolimer monomer besleme oranı ve molekül ağırlığının etkisi belirlenmiş; bu kopolimerlerin reoloji değiştiricileri olarak performansı rapor edilmiştir. Literatürde ilk kez i) kalsiyum alüminat çimento (CAC) ve ii) sıradan portland çimentosu-kireç haline getirilmiş kil-kalsiyum karbonat üçlü harmanları I) CAC'de yüksek yüzey gelişimi ve yüzey yükü ve ii) üçlü harmanlanmış çimentoda kalsine kil ve katı sülfat iyonlarının katmanlı yapısının karakteristik özelliklerini karşılayacak şekilde sentezlenmiştir. PCE'lerin i) alumina

süspansiyonlarının kesilme ve genleşmeli reolojik davranışları ve ii) yüksek yüklü alüminyum süspansiyonların imalatı ve katı dökme yeşil gövdelerin işlenmesi üzerine olan etkisi de araştırılmıştır. Hacimce %20 saf alumina süspansiyonları önemli miktarda partikül sıkışması gösterirken hacimce ve ağırlıkça% 1'den fazla kopolimer içeren %35 alumina süspansiyonları Newton davranışı göstermiştir. Bu süspansiyonlar, katı dökme yeşil gövdelerin imalatı için uygun bulunmuş ve işleme sürecinde malzemelerin önemli derecede uzaklaştırılabilmesini sağlamıştır.

ACKNOWLEDGEMENTS

I would like to express my sincere gratitude to my advisor, Prof. Ozge Akbulut, for the continuous support of my Ph.D and related studies, for her guidance, encouragement and immense knowledge. Thank you for being an inspiration and a role model for the rest of my life.

My special thanks go to Prof. Yusuf Menceloglu, Dean of the Faculty of Engineering and Natural Sciences, for his support and constructive comments and also Faculty of Engineering and Natural Sciences for providing this opportunity which allowed me to undertake this research.

I would like to thank my parents for supporting me spiritually throughout my PhD and my life in general.

Finally, my deepest gratitude and heartfelt thanks to my caring, loving, and supportive wife, Zahra, your encouragement when the times got rough are much appreciated. It was a great comfort and relief to know that you were always there for me.

TABLE OF CONTENT

List of Figures

Chapter 1 Extensional rheology and stability behavior of alumina suspensions in the presence of AMPS-modified polycarboxylate ether-based copolymers

This chapter is written based on the article “Extensional rheology and stability behavior of alumina suspensions in the presence of AMPS-modified polycarboxylate ether-based copolymers”. Here, we report the preparation and characterization of a new comb-type copolymer that includes acrylic acid (AA), 2-acrylamido-2-methylpropane sulfonic acid (AMPS), and polyethylene glycol-1000 (PEG-1000). Copolymers with different chemical formulations and molecular weights were synthesized by changing the reaction conditions and feed ratio. Capillary breakup extensional rheometer (CaBER) was used to investigate the effect of addition of copolymers on the extensional flow behavior of alumina suspensions. Rheological measurements revealed that addition of 1 wt. % of the copolymer with lowest molecular weight increases the maximum fraction of alumina particles in the system to 44 vol. % compared to 20 vol. % in pure alumina suspension.

1.1 Introduction

Water is the solvent of choice during ceramic powder processing since it is environmentally benign and cost-effective [1, 2]. Dispersion of colloidal ceramic particles in aqueous media is, therefore, critical for industrial processing such as frequently used casting, ink-jet printing [3], and spray drying [4]. Stable suspensions with high solid loadings (> 40 vol. %) [5] are desirable since obtaining sinterable and crack-free ceramic compact can hardly be achieved using suspensions with low solids contents. However, concentrated colloidal systems often show complex rheological behavior because of particle aggregation [6]. To obtain stable systems, dispersion of particles usually relies on prevailing of repulsive electrostatic force over Van der Waals force [7]. To impart charge on ceramic suspensions with high solid content, dispersants are used. Dispersants decrease the viscosity and agglomeration, homogenize the microstructure thus improve mechanical properties of the final product. The dispersant amount should be optimized since excess amounts can cause bridging flocculation whereas inadequate amounts lead to a reduction in absolute value of zeta potential [8-11].

Polyacrylic acid (PAA) is widely used in many systems [10-12] such as dispersion of Ti, Al_2O_3, and yttria-stabilized zirconia in aqueous media; but, performance of PAA is limited due to its simple structure. On the other hand, linear copolymers of PAA, depending on the types of synergistic functional groups, can provide various properties such as wider pH range for high absolute zeta potential value, lower optimum dosage of dispersant, and less sensitivity to flocculation in the presence of excess amount of dispersant [12-14]. The stabilizing effect of linear polymers can be improved by addition of side chains in order to harness steric hindrance effect as well. These amphipathic structures are usually composed of long hydrophilic side chains grafted to a backbone. The backbone bears ionizable groups such that they can anchor to the surface of particles while side chains protrude into the medium and produce steric hindrance effect [1, 2, 7]. Bouhamed *et al*. [1] confirmed the stabilizing effect of 2-acrylamido-2-methylpropane sulfonic acid-polyethyleneglycol methacrylate copolymers at 30 vol. % alumina suspension. Ran *et al*. [15] reported poly (styrene-co-maleic anhydride)-methoxy polyethylene glycol copolymer as an effective dispersant to reduce viscosity of suspension with ~30 vol. % alumina particles. The performance of dispersants in these systems is usually evaluated by rotational rheometry. However, many applications of ceramic suspensions such as ink-jet printing [3], ink-jet deposition in microchannels [16], and spray drying [4] necessitate visco-elasto-capillary characterization of these suspensions. The elongational behavior of the drop of suspension can be studied by CaBER since it can determine the extensional properties of the drop before the pinch-off point [17].

1.2 Characterization of copolymers

The esterification of PEG-1000 was carried out by maleic anhydride via the procedure that was proposed in literature [18]. This product was used for polymerization without any purification. Choosing PEG-1000 for esterification was based on the higher dispersing ability of AMPS/PEG-1100 copolymer than AMPS/PEG-2000 [19]. Different polycarboxylate ether-based AA/AMPS/PEGMA copolymers were synthesized based on a method described by Salami and Plank [20]; these are named from PCE1 to PCE6 in Table 1.1. As a reference, we also synthesized AA/AMPS linear copolymer referred as PC in Table 1.1.

Table 1.1 Molar compositions of starting materials for polymerization

	Molar ratio	
Polymer	AA/AMPS/ PEGMA	pH
PCE1	25/25/1	6
PCE2	25/25/1	8
PCE3	25/25/1	13
PCE4	10/40/1	8
PCE5	20/30/1	8
PCE6	30/20/1	8
PC	25/25/0	6

Chemical structure of copolymers was characterized by using H^1-NMR (Figure 1.1). Proton chemical shifts were observed at δ 1.5, 1.7, 2.1, 3.4 and 3.7 ppm that are attributed to $–CH_3$ group of AMPS (5), $–CH_2$ (2) and –CH (1) groups in main chain of polymer, $–CH_2$ group of AMPS (4), and $–CH_2CH_2–O$ group of PEG chain (3), respectively.

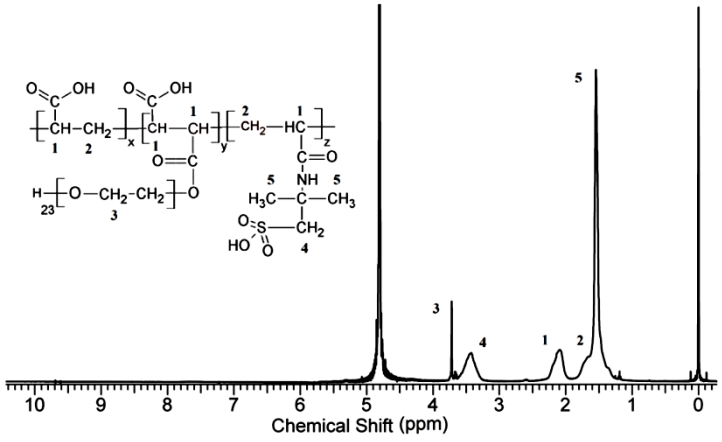

Figure 1.1 H^1-NMR of PCE2

Dilute solution viscometry was used to confirm the polymerization of copolymers with different molecular weights. Figure 1.2 shows reduced viscosity of the copolymers as a function of concentration. Expectedly, AA/AMPS copolymer exhibited the lowest intrinsic viscosity (1.7 dl/g) while PCE1, PCE2, and PCE3 display the 4.3, 3.1 and 5.4 dl/g,

respectively. Thus, we concluded that the molecular weight of PCE2 is the lowest among the comb type copolymers.

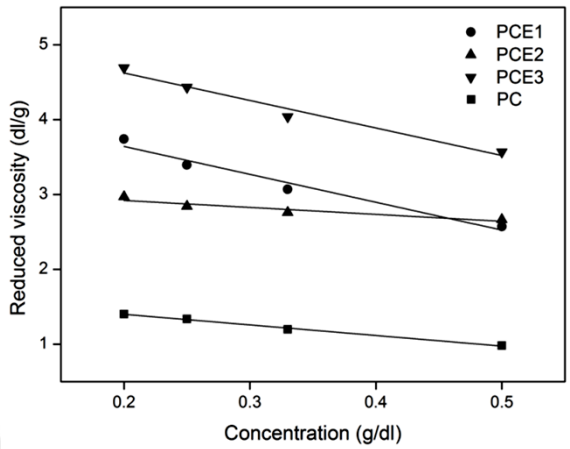

Figure 1.2 Dilute solution viscometry of selected polymers synthesized at different pH values

1.3 Characterization of diluted suspension

1.3.1 Adsorption of copolymers and electrokinetic study

Figure 1.3a shows the adsorption isotherms of different copolymers at native pH (7–8) of alumina suspensions. The amount of adsorbed copolymers increases significantly with initial amount and then stabilizes near a plateau value that is typical for a monolayer adsorption isotherm [21]. This plateau is reached at higher amounts when the molecular weight of copolymers increases (PCE3 > PCE1 > PCE2). Figure 1.3b is a representative result of TGA on dried alumina suspensions that contain different amounts of copolymer PCE2. Increasing amount of initial copolymer raised the amount of weight loss. This result, in parallel with the results of adsorption isotherm test, indicated that increasing amount of copolymers in suspensions increase the amount of strongly adsorbed copolymers on the surface of alumina particles.

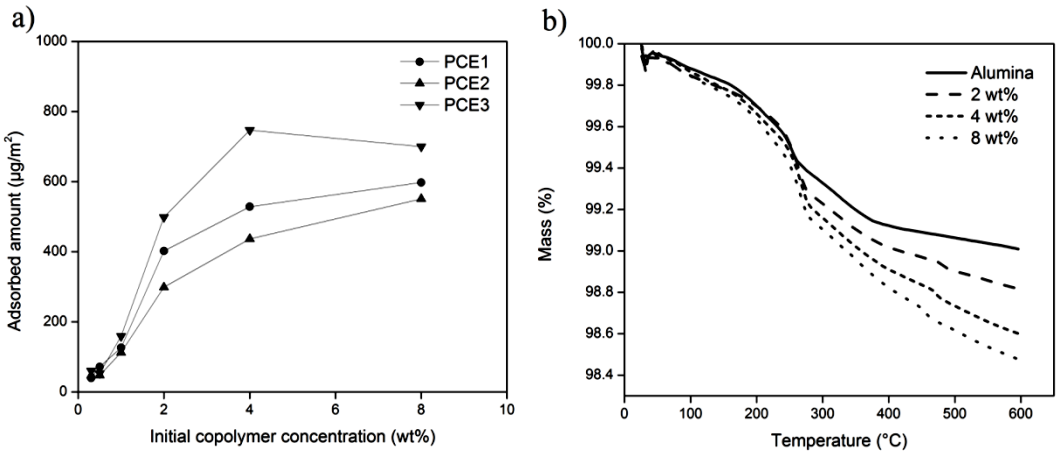

Figure 1.3 a) Adsorption isotherms of different copolymers on alumina particles and b) TGA of dried alumina suspensions including different amounts of PCE2

Given the importance of the electrokinetic behavior of suspensions for interpreting the adsorption behavior and also change of rheological properties in the presence copolymers, the effect of pH on zeta potential of alumina suspensions was given in Figure 1.4. A representative result of zeta potential measurement that was carried out on alumina suspensions with different amounts of PCE2 was given in Figure 1.4a. Isoelectric point (IEP) of pure alumina suspension is ~8 indicating that the surface of alumina particles hold Al–OH bonds and positively charged sites of $Al–OH_2^+$ between pH 7 and 8. Adsorption of the copolymer to surface of the particles shifts the IEP to lower pH values. Carboxylate and sulfonate groups are reported to be adsorbed on the surface of alumina particles by making bonds with $Al–OH_2^+$ ions [2, 10]. The inclusion of the copolymer results in bonding between ionized functional groups, (COO^- and SO_3^-) and $Al–OH_2^+$ sites. Consequently, positively charged alumina particles are covered with negatively charged copolymers as shown by IEP shifting to lower pH values. At higher than 0.3 wt. % copolymer, the number of negative charges introduced by the copolymer surpasses the number of positively charged sites and changing the sign of zeta potential values takes place as a result of this overcompensation phenomenon [22]. Figure 1.4b illustrates the zeta potential values in the presence of 0.5 wt. % and 2 wt. % of different copolymers. PCE1 and PCE2 display almost identical electrokinetic behavior while maximum absolute value of zeta potential was detected in the suspension containing PCE3. The latter observation can be attributed to the

higher number of ionized groups in the backbone of PCE3 due to its higher molecular weight.

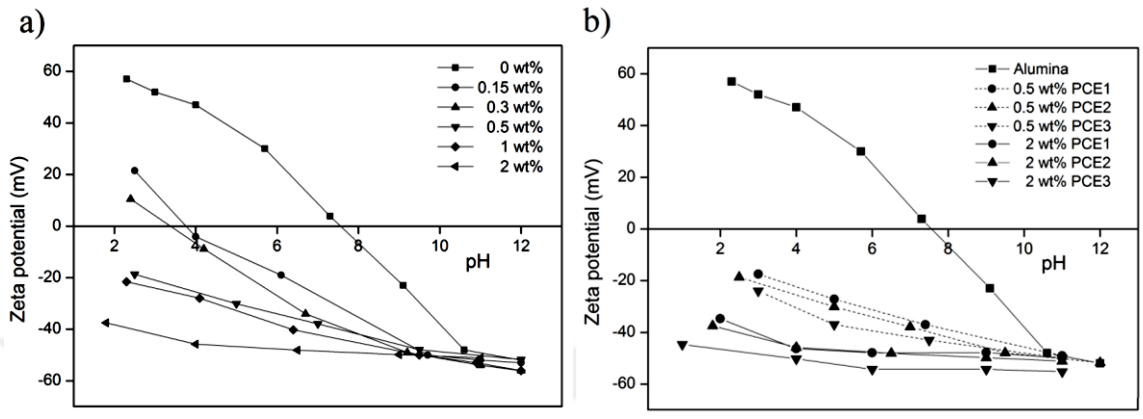

Figure 1.4 Effect of pH on zeta potential of the alumina suspensions in the presence of a) different amount of PCE2, and b) 0.5 wt. % and 2 wt. % of different copolymers

Analysis of electrokinetic behavior of suspensions in the presence of PCE1 and PCE2 is helpful to understand the conformation of adsorbed copolymers. Affinity of both copolymers to the surface of alumina particles is close to each other since the curves that they generate in zeta potential versus pH graph are superimposable (Figure 1.4b). However, according to adsorption isotherm test, more PCE1 is adsorbed on the surfaces of alumina particles; hence, we speculate that not all parts of the main chain of copolymers are adsorbed and copolymers adopt a loop structure on the surface of particles [23]. Furthermore, this loop conformation explains the difference among the amounts of adsorbed copolymer in plateau region in adsorption isotherm test (Figure 1.3a). A fraction of backbone of a copolymer with no bonding to the surface increases the amount of adsorbed copolymer. When molecular weight of copolymers increases, a rise in the length of copolymers with no bonding is inevitable. Given the certain number of sites on the surface of the particles available for adsorption, higher amount of adsorbed copolymer in plateau region with increasing molecular weight of copolymer (PCE3 > PCE1 > PCE2) is expected.

1.3.2 Stability

Figure 1.5a shows change in hydrodynamic radius (r_h) of alumina particles with time in 4 wt. % alumina suspensions and 2 wt. % of different copolymers compared to alumina particles at pH 7.5. Choosing 2 wt. % copolymers was based on the fact that all copolymers reach saturation plateau at 2 wt. % (Figure 1.4b). Pure alumina suspension displayed r_h of 350 nm initially and 390 nm after 10 min due to the formation of aggregated colonies. Since zeta potential of pure alumina suspension at this pH is around 5 mV (Figure 1.4), repulsive interactions among particles are not sufficient to prevent agglomeration. On the other hand, in the presence of 2 wt. % copolymers, initial r_h of 117, 116, and 121 nm were observed in suspensions containing PCE1, PCE2, and PCE3, respectively (Figure 1.5a).

We based stability measurements on a procedure proposed by Cynthia *et al*. [24] Since no discrete layer was observable during gravity settling, we used the time needed for 25% mass removal of alumina particles at sampling height (height of 60 ml in 100 ml graduated cylinder). In the absence of copolymers, alumina suspension reached 75% of initial concentration at sampling height in 25 min while suspensions that contain PCE1, PCE2, and PCE3 necessitated 90, 110, and 35 min, respectively. This observation indicates the higher stability of suspensions in the presence of copolymers and is also consistent with the results of r_h measurements (Figure 1.5a). In the absence of sufficient repulsive forces in pure alumina suspensions that is evidenced by low zeta potential value (Figure 1.4), attractive van der Waals force prevails over interparticle interactions [25] and aggregated colonies with particle size of ~400 nm are formed (Figure 1.5a). Hence, formation of these clusters decreased the time of sedimentation and caused higher mass removal of particles compared to well-dispersed particles in the presence of copolymers.

To determine the lowest amount of copolymer that is needed for further rheological measurements, we measured particle size distribution of suspensions containing different amounts of PCE2 15 minutes after sonication (Figure 1.5b). PCE2 was chosen since it shows the highest dispersing ability and stability among all copolymers. Sample with 0.3 wt. % PCE2 displays a low intensity peak at particle size of 1 µm in addition to the main peak centered at 110 nm. Appearance of this small peak can be described by incomplete surface coverage of 0.3 wt. % PCE2. Addition of 0.5 wt. % PCE2 led to disappearance of

this small peak and observation of a single population curve centered at ~120 nm; hence, we concluded that 0.5 wt. % is the minimum amount of PCE2 needed to stabilize alumina suspensions for further rheological tests.

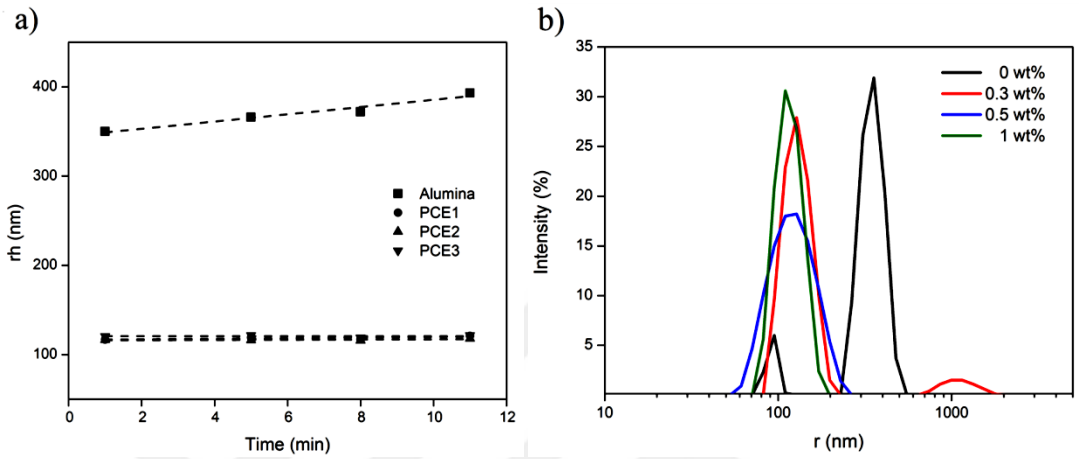

Figure 1.5 a) Change in rh of alumina particles with time in suspensions with and without 2 wt. % copolymers and b) particle size distribution of suspensions after 15 minutes in the presence of different amounts of PCE2

1.4 Rheological measurements

We present the change of midpoint diameter in 20 vol. % (~50 wt. %) alumina suspension thread as a function of time in Figure 1.6a. In the absence of any additives, this 20 vol. % solid content was found to be the highest amount of alumina for preparation of a suspension. As seen in Figure 1.6a, pure alumina suspension exhibits Newtonian behavior in low deformation times, characterized by linear necking rate in time that is followed by exponential decrease of midpoint diameter until the break up point. The deformation imposed on the fluid can be described by Hencky strain, $\varepsilon = 2\ln D_0/D(t)$, where D_0 is the plate diameter (mm). Figure 1.6b shows extensional viscosity of pure alumina suspension as a function of Hencky strain. The apparent transient extensional viscosity (η_E) of stretching fluid can be calculated as:

$$\eta_E = \frac{\Delta\tau(t)}{\dot{\varepsilon}(t)} = -\frac{\sigma}{D(t)/dt} \qquad (1)$$

where $\Delta\tau(t)$ is the total extensional stress difference in elongating flow (Pa), $\dot{\varepsilon}(t)$ is instantaneous strain rate (s^{-1}), and σ is the fluid surface tension (N/m) [26]. Without

inclusion of additives, pure alumina suspension displays a severe strain-hardening behavior and extensional viscosity diverges to maximum value of approximately 2,000 Pa.s. Since, alumina particles hold low surface charge in the native pH of alumina suspension, dominancy of Van der Waals attraction among particles results in particle flocculation. Thus, we postulated that the non-Newtonian stress contribution, generated by flocculation of particles, to total stress evolution retarded the necking rate of the thread. This behavior resembles the creation of a connected 3D network of aggregates beyond the percolation threshold [23], which similarly increases the viscosity asymptotical to infinity.

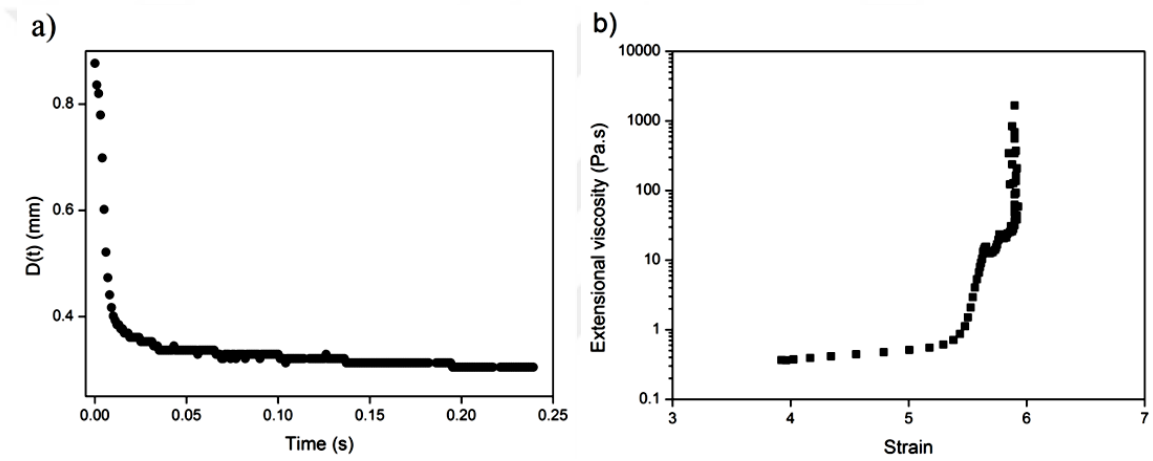

Figure 1.6 a) Change of midpoint diameter as a function of time and b) extensional viscosity as a function of strain in 20 vol. % alumina suspension

1.4.1 Effect of AA/AMPS ratio on the rheological behavior

After inclusion of different copolymers even at 0.3 wt. %, 20 vol. % alumina suspensions showed high necking rates—the viscosity has decreased significantly such that change of midpoint diameter was not traceable by the laser micrometer. Consequently, we increased the solid content of suspensions to 35 vol. % (~68 wt. %). Figure 1.7a and Figure 1.7b show the change of midpoint diameter in time and extensional viscosity as a function of Hencky strain, respectively, in the samples containing 0.5 wt. % of different copolymers. Presence of copolymers with different AA/AMPS ratio changed the extensional flow behavior of alumina suspensions, that is, Newtonian behavior in low deformation time followed by elastocapillary thinning region before the break up point (Figure 1.6a). As seen in Fig 7b, all samples except the one with PCE2 display a modest strain hardening before break up point. Increase of AA/AMPS ratio from 0.25 in PCE4 to 1 in PCE2 resulted in

disappearance of strain hardening while further increase of AA/AMPS ratio to 1.5 (PCE6) led to observation of strain hardening in these samples.

For a model viscoelastic fluid, elastocapillary thinning region—the region before the break up point, can be described by an exponential decay of the midpoint diameter in time for $t > t_1$ as shown in eq. 2 [27]:

$$\frac{D(t)}{D_0} = \left(\frac{G_1 D_0}{4\sigma}\right)^{1/3} \exp\left(-\frac{t-t_1}{3\lambda_e}\right) \quad (2)$$

where G_1 is related to elastic modulus, t_1 (s) is the onset of elastocapillary region, and λ_e is the longest fluid relaxation time (s^{-1}). Fitting experimental points in elastocapillary thinning region in Figure 1.7a with eq. 2 indicated that the increase of AA/AMPS ratio from 0.25 in PCE4 to 1 in PCE2 reduces the relaxation time (λ_e) of suspension from 1.9 ms to 1.2 ms. Further increase of AA/AMPS ratio to 1.5 in PCE6 raised the λ_e to 3.1 ms. In addition to the deflocculating effect of copolymers, change in extensional flow behavior can be attributed to the increase in the fast motion of alumina particles as a result of the lower attraction between particles. We, therefore, concluded that using AA/AMPS ratio of 1 leads to the highest synergistic effect of functional groups as indicated by the smallest relaxation time.

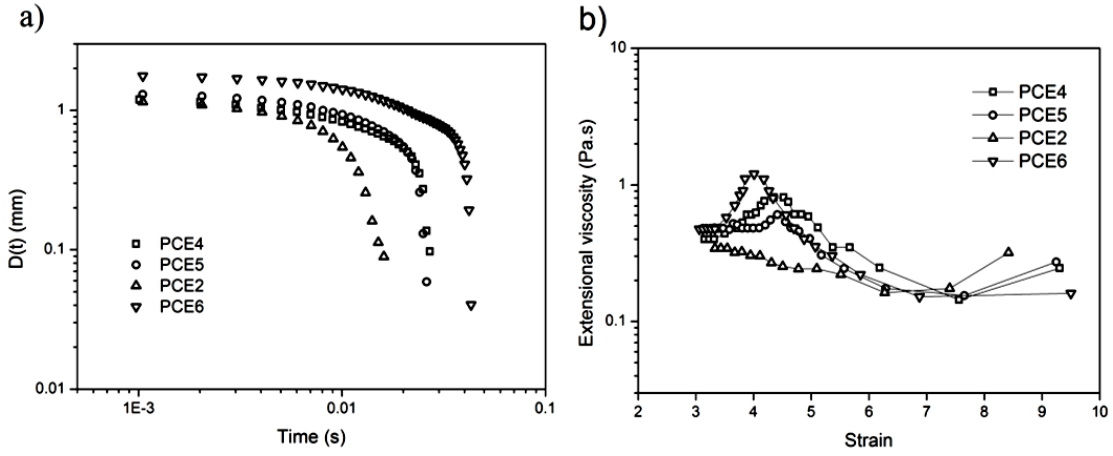

Figure 1.7 a) Change of midpoint diameter as a function of time and b) extensional viscosity as a function of Hencky strain for samples with 0.5 wt. % PCEs

1.4.2 The effect of molecular weight of copolymers on the rheological behavior

We also investigated the effect of molecular weight of the copolymers on extensional flow of suspensions. Among the polymers with AA/AMPS ratio of 1 (PCE1, PCE2, and PCE3), we first plotted extensional viscosity of 35 vol. % alumina suspensions in Figure 1.8a as a function of Hencky strain for samples containing increasing amounts of PCE2. Pure Alumina suspension with 20 vol. % solid content was also used the reference sample for comparison. Addition of 0.3 wt. % PCE2 decreases the strain hardening behavior while thinning is observed in the presence 0.4 and 0.5 wt. % copolymer (Figure 1.8a). These observations are indicative of the presence of interparticle interactions in the system [28]. In addition, deviation from Newtonian behavior is minimal in the suspension with 1 wt. % copolymer due to the significant decrease of interparticle attraction that is in agreement with zeta potential measurements. We, then, studied the extensional viscosity of alumina suspensions as a function of Hencky strain in the presence of copolymers with different molecular weights (Figure 1.8b). Alumina suspension that contains the copolymer with the highest molecular weight (PCE3) displayed the highest extensional viscosity and modest strain hardening effect. Decrease of molecular weight led to reduction of extensional viscosity and disappearance of the strain hardening region. These results can be explained by the effect of adlayer thickness on the effective volume fraction (ϕ_{eff}) and effective particle distance (2Λ) in suspensions.

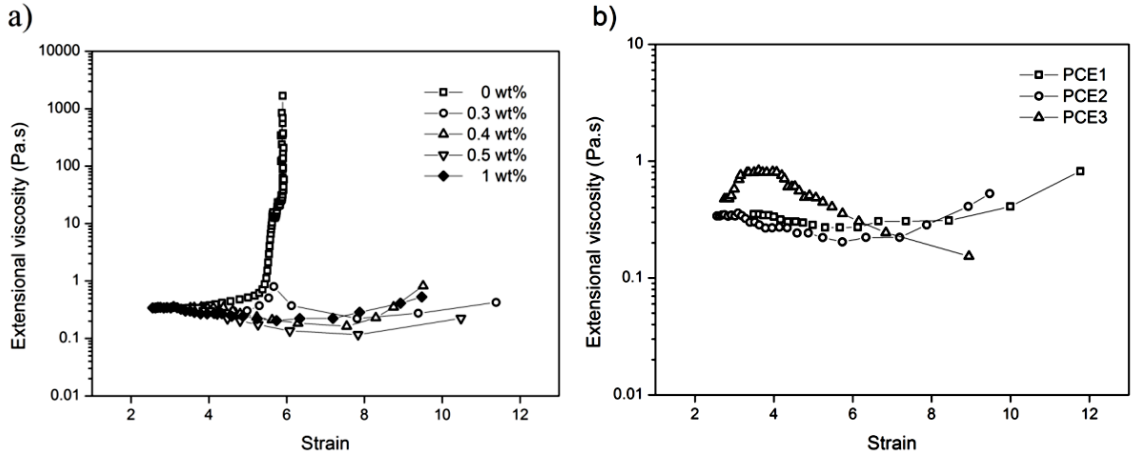

Figure 1.8 Extensional viscosity of 35 vol. % alumina suspension as a function of Hencky strain for samples with a) different wt. % of PCE2 and b) 1 wt. % of copolymers with different molecular weight

The effective volume fraction of solids in suspension ($\phi_{eff} = \phi\left[1 + \frac{\delta}{a}\right]^3$) consists of the real volume fraction (ϕ) of particles with radius of (a) and the excluded volume formed by the stabilizing adlayer with thickness of (δ). This adlayer should be sufficiently thick in order to prevent agglomeration and also thin enough to minimize the excluded volume [29]. Presence of this excluded volume reduces the interparticle distance, which can be estimated by ($\frac{\Lambda}{r} = [\frac{\phi_m}{\phi_{eff}}]^{\frac{1}{3}} - 1$), where ϕ_m is the maximum packing fraction of monodisperse spherical particles (0.638 for random packing) [30]. Using the difference between the hydrodynamic radius of the coated and bare alumina particle as the polymer adlayer thickness [31], effective volume fraction and effective interparticle distance were calculated (Table 1.2).

Table 1.2 Effective volume fraction and effective interparticle distance of alumina particles in the presence of 1 wt. % copolymers with different molecular weight

copolymer	δ (nm)	ϕ_{eff}	2Λ (nm)
PCE1	7	0.42	33
PCE2	6	0.41	35
PCE3	11	0.47	24

As seen in Table 1.2, presence of PCE3 reduces the interparticle distance to 24 nm, which is in the range of adlayer thickness ($\delta \sim \Lambda$). Therefore, the strain hardening behavior observed in this suspension potentially results from the interaction of copolymers. On the other hand, decrease of molecular weight (PCE1 and PCE2) led to lower δ and higher Λ such that the system can incorporate higher volume fraction of alumina particles.

1.4.3 Maximum volume fraction of alumina in suspensions

Figure 1.9a shows the change of midpoint diameter in time for samples with 1 wt. % PCE2 and increasing amount of alumina particles to find the maximum volume fraction (ϕ_{max}) of the dispersed phase. We chose 1 wt. % PCE2 based on the fact that deviation from Newtonian behavior is minimal in the suspension with 1 wt. % copolymer (Figure 1.8). To describe the time evolution of the neck diameter, we used the power-law fluid expression, that is, the midpoint diameter changes as:

$$\frac{D(t)}{D_0} = \phi(n)(\frac{\sigma}{K})(t_c - t)^n \quad (3)$$

where n is the power-law exponent, K is the consistency index and $\phi(n)$ is a numerically determined factor [26]. The suspension with 30 vol. % alumina particles ruptured in less than 0.02 s while increasing amount of particles retarded the onset of elastocapillary region (t_1). The onset is found by intersection point of the lines that are fitted to linearly decaying regime and exponentially decaying regime of elastocapillary region [27]. By fitting experimental points to the power-law fluid expression in eq. 3 and elastocapillary region to eq. 2, the fitting parameters were calculated as shown in Table 1.3.

Table 1.3 Onset of elastocapillary region (t_1), relaxation time (λ_e), and power-law exponent of suspensions (n) with 1 wt. % PCE2 at increasing amounts of solid volume fraction (ϕ)

ϕ	t_1 (ms)	λ_e (ms)	n
0.30	12	0.8	1.00
0.35	17	1.1	0.99
0.375	35	1.5	0.95
0.40	180	4.1	0.85

Figure 1.9b shows extensional viscosity of suspensions with 1 wt. % PCE2 as a function of Weissenberg number ($\lambda_e.\dot{\varepsilon}$) that is used to horizontally collapse the results. Increasing solid volume fraction shifted the extensional viscosity curve to higher values and led to observation of thinning behavior above 35 vol. %. Change of flow behavior from well-dispersed system in 30 vol. % to flocculated system in 40 vol. % is also evidenced by reduction of n from 1, which is the characteristic value for Newtonian fluid, to n=0.85.

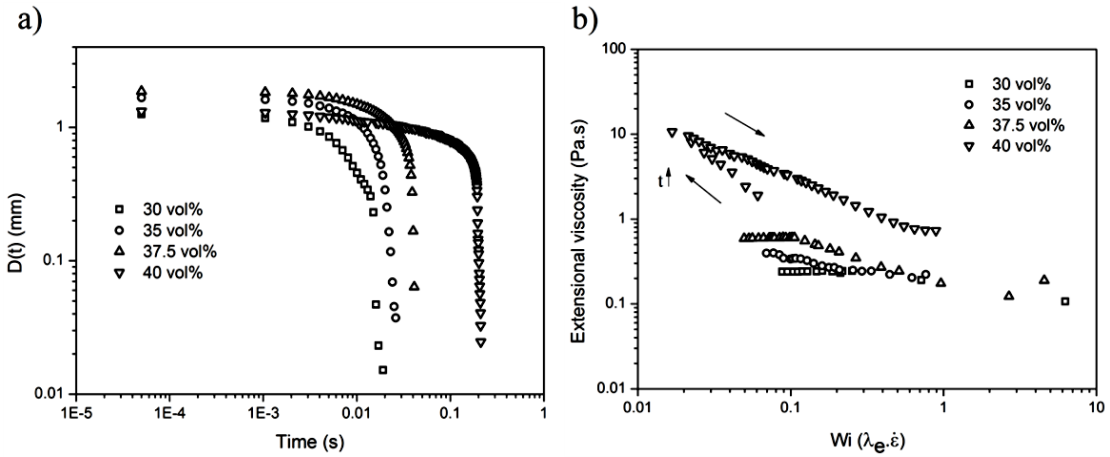

Figure 1.9 a) Change of midpoint diameter as a function of time and b) extensional viscosity as a function of Weissenberg number for increasing vol. % of alumina suspensions with 1 wt. % PCE2.

The suspension with 40 vol. % alumina particles initially showed decrease of strain rate towards the maximum extensional viscosity (η_{max}) and subsequently, decrease of extensional viscosity was observed with increasing strain rate, as shown in the Figure 1.9b with arrows. On the other hand, the suspension with 45 vol. % alumina particles only showed the region of decreasing strain rate towards η_{max} (Figure 1.10). Similar CaBER response was reported by White *et al.* [32] for 35 vol. % cornstarch-water suspensions. They suggested that possibly the compressive flow in the radial direction is increasing the packing of particles locally and facilitating the jamming of particles or clusters.

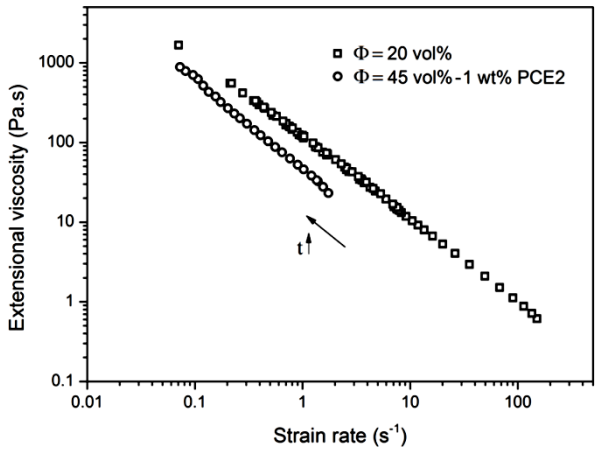

Figure 1.10 Extensional viscosity as a function of strain rate for 20 vol. % pure alumina suspension and for 45 vol. % alumina suspension containing 1 wt. % PCE2

In Figure 1.11, we present the change in extensional viscosity and relaxation time of alumina suspensions as a function of particle volume fraction. All suspensions contained 1 wt. % PCE2 and extensional viscosity was obtained at $\lambda_e\dot{\varepsilon}$=0.08. As particle fraction increases above 30 vol. %, viscosity and relaxation times of suspensions gradually increases up to 37.5 vol. % and grow significantly beyond this point. Rapid increase of λ_e and η_E towards maximum volume fraction of dispersed phase is an indication of pronounced elasticity and formation of network of aggregates.

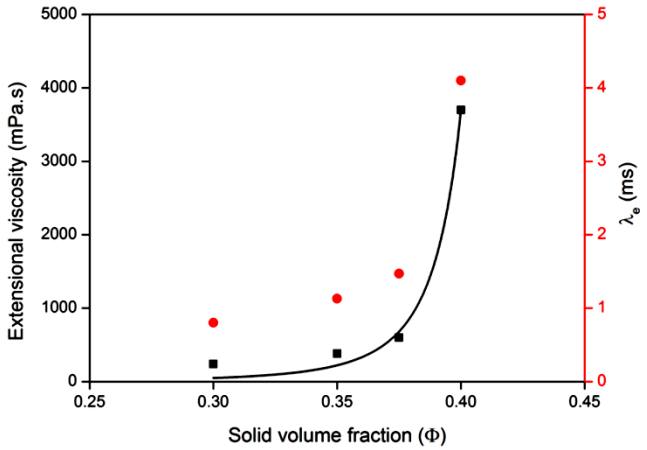

Figure 1.11 Dependency of viscosity at $\lambda_e\dot{\varepsilon}$ = 0.08 and relaxation time on the volume fraction of alumina particles in the presence of 1 wt. % PCE2

Dependency of the extensional viscosity on volume fraction of alumina particles is analogous to that of the shear viscosity on volume fraction of dispersed phase [23, 33]. This dependency could be fitted by Kreiger-Dougherty equation as:

$$\eta = \eta_0\left(1 - \frac{\phi}{\phi_{max}}\right)^{-[\eta]\phi_{max}} \quad (4)$$

where η_0 is the viscosity of liquid medium (Pa.s) and [η] is the intrinsic viscosity [34]. However, the presence of copolymer adlayer increases the volume fraction of dispersed phase. In order to take into account the effect of higher ϕ_{eff} compared to ϕ on viscosity, we used modified Kreiger-Dougherty model ($\eta = \eta_0\left(1 - \frac{\phi_{eff}}{\phi_{max}}\right)^{-[\eta]\phi_{max}}$). By satisfactory fitting of the experimental points with modified Kreiger-Dougherty equation, ϕ_{max} of 44% and [η] of 5.6 were obtained, which are consistent with reported values in

literature [23]. Moreover, ϕ_{max} of 44% is in agreement with the 45% that we found experimentally (Figure 1.10).

1.5 Conclusion

Particle size analysis and rheological measurements confirmed the stabilizing effect of copolymers and we showed that the maximum amount of alumina that can be fed into the suspension is ~45 vol. % at 1 wt. % copolymer (PCE2) addition. The effect of copolymers in reducing extensional viscosity and elimination of strain hardening behavior in alumina suspensions suggests a strong potential for these copolymers to be used in applications like ink-jet printing, 3D printing, and spraying.

1.6 Reference

[1] H. Bouhamed, S. Boufi, A. Magnin, Alumina interaction with AMPS-MPEG copolymers produced by RAFT polymerization: stability and rheological behavior, J Colloid Interf Sci, 333 (2009) 209-220.
[2] H. Bouhamed, A. Magnin, S. Boufi, Alumina interaction with AMPS-MPEG random copolymers III. Effect of PEG segment length on adsorption, electrokinetic and rheological behavior, J Colloid Interf Sci, 298 (2006) 238-247.
[3] K.A.M. Seerden, N. Reis, J.R.G. Evans, P.S. Grant, J.W. Halloran, B. Derby, Ink-Jet Printing of Wax-Based Alumina Suspensions, J Am Ceram Soc, 84 (2001) 2514-2520.
[4] A. Schrijnemakers, S. Andre, G. Lumay, N. Vandewalle, F. Boschini, R. Cloots, B. Vertruyen, Mullite coatings on ceramic substrates: Stabilisation of Al2O3-SiO2 suspensions for spray drying of composite granules suitable for reactive plasma spraying, J Eur Ceram Soc, 29 (2009) 2169-2175.
[5] A.R. Studart, E. Amstad, L.J. Gauckler, Colloidal stabilization of nanoparticles in concentrated suspensions, Langmuir : the ACS journal of surfaces and colloids, 23 (2007) 1081-1090.
[6] S. Mohanty, B. Das, S. Dhara, Poly(maleic acid) – A novel dispersant for aqueous alumina slurry, Journal of Asian Ceramic Societies, 1 (2013) 184-190.
[7] C.P. Whitby, P.J. Scales, F. Grieser, T.W. Healy, G. Kirby, J.A. Lewis, C.F. Zukoski, PAA/PEO comb polymer effects on rheological properties and inter-particle forces in aqueous silica suspensions, J Colloid Interf Sci, 262 (2003) 274-281.
[8] C.J. Tsai, C.N. Chen, W.J. Tseng, Rheology, structure, and sintering of zirconia suspensions with pyrogallol-poly(ethylene glycol) as polymeric surfactant, J Eur Ceram Soc, 33 (2013) 3177-3184.
[9] P.S. Bhosale, J.C. Berg, Poly(acrylic acid) as a rheology modifier for dense alumina dispersions in high ionic strength environments, Colloid Surface A, 362 (2010) 71-76.
[10] Y. Liu, L. Gao, Dispersion of aqueous alumina suspensions using copolymers with synergistic functional groups, Mater Chem Phys, 82 (2003) 362-369.

[11] R.G. Neves, B. Ferrari, A.J. Sanchez-Herencia, C. Pagnoux, E. Gordo, Role of stabilisers in the design of Ti aqueous suspensions for pressure slip casting, Powder Technol, 263 (2014) 81-88.
[12] Y. Liu, L. Gao, Deflocculation study of aqueous nanosized Y–TZP suspensions, Mater Chem Phys, 78 (2003) 480-485.
[13] C. Xiao, L. Gao, M. Lu, H. Chen, L. Guo, L. Tao, Synergistic effect of copolymer and poly(vinylpyrrolidone) mixtures on rheology of aqueous SiC suspensions, Colloid Surface A, 355 (2010) 104-108.
[14] T.S. Liao, C.L. Hwang, Y.S. Ye, K.C. Hsu, Effects of a carboxylic acid/sulfonic acid copolymer on the material properties of cementitious materials, Cem Concr Res, 36 (2006) 650-655.
[15] Q.P. Ran, M. Qiao, J.P. Liu, C.W. Miao, SMA-g-MPEG comb-like polymer as a dispersant for Al2O3 suspensions, Appl Surf Sci, 258 (2012) 2447-2453.
[16] A.K. Mogalicherla, S. Lee, P. Pfeifer, R. Dittmeyer, Drop-on-demand inkjet printing of alumina nanoparticles in rectangular microchannels, Microfluid Nanofluid, 16 (2014) 655-666.
[17] O.A. Basaran, Small-scale free surface flows with breakup: Drop formation and emerging applications, AIChE J, 48 (2002) 1842-1848.
[18] S.H. Lu, G. Liu, Y.F. Ma, F. Li, Synthesis and Application of a New Vinyl Copolymer Superplasticizer, J Appl Polym Sci, 117 (2010) 273-280.
[19] A. Buyukyagci, G. Tuzcu, L. Aras, Synthesis of copolymers of methoxy polyethylene glycol acrylate and 2-acrylamido-2-methyl-1-propanesulfonic acid: Its characterization and application as superplasticizer in concrete, Cem Concr Res, 39 (2009) 629-635.
[20] O.T. Salami, J. Plank, Synthesis, effectiveness, and working mechanism of humic acid-{sodium 2-acrylamido-2-methylpropane sulfonate-co-N,N-dimethyl acrylamide-co-acrylic acid} graft copolymer as high-temperature fluid loss additive in oil well cementing, J Appl Polym Sci, 126 (2012) 1449-1460.
[21] R.I. Masel, Principles of adsorption and reaction on solid surfaces, John Wiley & Sons, 1996.
[22] H. Bouhamed, S. Boufi, A. Magnin, Dispersion of alumina suspension using comb-like and diblock copolymers produced by RAFT polymerization of AMPS and MPEG, J Colloid Interface Sci, 312 (2007) 279-291.
[23] H. Bouhamed, S. Boufi, A. Magnin, Alumina interaction with AMPS-PEG random copolymer II. Stability and rheological behavior, Colloid Surface A, 253 (2005) 145-153.
[24] C.R. Evanko, R.F. Delisio, D.A. Dzombak, J.W. Novak Jr, Influence of aqueous solution chemistry on the surface charge, viscosity and stability of concentrated alumina dispersions in water, Colloid Surface A, 125 (1997) 95-107.
[25] W.J. Tseng, C.H. Wu, Sedimentation, rheology and particle-packing structure of aqueous Al2O3 suspensions, Ceram Int, 29 (2003) 821-828.
[26] G.H. McKinley, Visco-elasto-capillary thinning and break-up of complex fluids, British Society of Rheology 2005.
[27] S.J. Haward, V. Sharma, C.P. Butts, G.H. McKinley, S.S. Rahatekar, Shear and Extensional Rheology of Cellulose/Ionic Liquid Solutions, Biomacromolecules, 13 (2012) 1688-1699.
[28] C. Viebke, J. Meadows, J.C. Kennedy, P.A. Williams, Effect of soluble polymers on the shear and extensional viscosity characteristics of a concentrated latex dispersion, Langmuir : the ACS journal of surfaces and colloids, 14 (1998) 1548-1553.

[29] W.M. Sigmund, N.S. Bell, L. Bergstrom, Novel powder-processing methods for advanced ceramics, J Am Ceram Soc, 83 (2000) 1557-1574.
[30] S. Jain, J.G.P. Goossens, G.W.M. Peters, M. van Duin, P.J. Lemstra, Strong decrease in viscosity of nanoparticle-filled polymer melts through selective adsorption, Soft Matter, 4 (2008) 1848-1854.
[31] G.K. Min, M.A. Bevan, D.C. Prieve, G.D. Patterson, Light scattering characterization of polystyrene latex with and without adsorbed polymer, Colloid Surface A, 202 (2002) 9-21.
[32] E.E.B. White, M. Chellamuthu, J.P. Rothstein, Extensional rheology of a shear-thickening cornstarch and water suspension, Rheol Acta, 49 (2009) 119-129.
[33] A. Rincon, A.S.A. Chinelatto, R. Moreno, Tape casting of alumina/zirconia suspensions containing graphene oxide, J Eur Ceram Soc, 34 (2014) 1819-1827.
[34] I.M. Krieger, T.J. Dougherty, A mechanism for non-Newtonian flow in suspensions of rigid spheres, Tran Soc Rheol, 3 (1959) 137-152.

Chapter 2 A PCE-based rheology modifier allows machining of solid cast green bodies of alumina

This chapter is written based on the article "A PCE-based rheology modifier allows machining of solid cast green bodies of alumina". Here, we show the feasibility of the casting of aqueous alumina suspensions through the use of a PCE-based superplasticizer synthesized at pH 8 with monomer feed ratio of 25/25/1 (AA/AMPS/PEGMA). These conditions were chosen based on the superplasticizing ability of the copolymer compared to that of copolymers with different chemical and structural compositions (chapter 1). We drilled the solid-cast cylindrical bodies without visible cracks and obtained terraced structures with smooth surfaces. This system does not necessitate binders to sustain its strength and therefore, the binder burnout step is eliminated from the process.

2.1 Introduction

Solid casting is the method of choice for the production of several ceramic objects from laboratory crucibles to turbine blades since it is scalable, simple and necessitates only low cost capital investment [1, 2]. In general, for further shaping of solid cast and then sintered bodies, only limited post-sintered machining, such as grinding, can be used due to high hardness and low toughness of these objects [3]. On the other hand, machining of the green body can i) allow additional machining processes, such as milling, drilling, and lathing to be implemented , ii) increase production speed due to faster material removing rates, and iii) eliminate early tool wear and possible crack formations [4-6]. Therefore, for cost-effective and simple fabrication of ceramics, there is a need for developing systems that can produce green bodies with enough strength to withstand machining. In solid casting, high particle loadings and well-packing is necessary to produce high strength green bodies; however, at higher loadings the viscosity increases and homogeneity of the slurry decreases significantly [7].

2.2 Rheological characterization

In general, viscosities in the range of 0.3–10 Pa.s were found to work well with solid casting and shear rates of 1–100 s^{-1} are frequently encountered in the process [8-10]. Lower viscosities result in well-packed green bodies that is necessary to produce high strength

structures [11]. We monitored the shear viscosity of 35 wt. % alumina suspensions in the presence of 1–4 wt. % superplasticizer at the shear rate of 1 s^{-1} (Figure 2.1a). The viscosity exhibited a sharp drop at 1.25 wt. % addition of the superplasticizer. This kind of dip in the viscosity of PCE-based copolymers was shown to arise from steric contribution of PEG side chains and ionic charge in the backbone of the copolymers [12, 13]. Also, at 35 vol. % alumina loading, the system with 1.25 wt. % superplasticizer displayed lowest shear thinning behavior manifested by the lowest slope in viscosity versus shear rate graph indicating better dispersion of alumina particles (Figure 2.1b) [14].

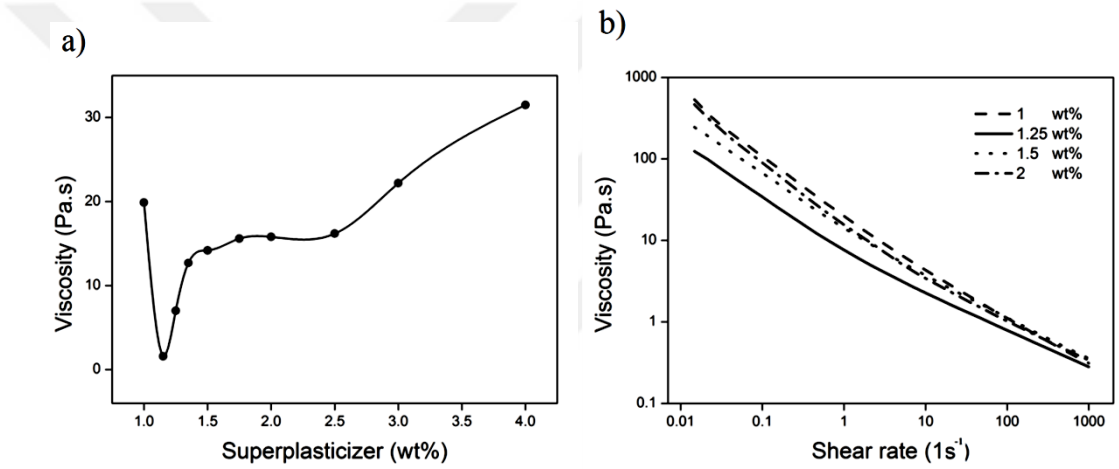

Figure 2.1 a) Viscosity of 35 vol. % alumina suspensions in the presence of 1–4 wt. % superplasticizer at shear rate of 1 s^{-1}, b) dependence of viscosity to shear rate at 35 vol. % alumina suspensions with different amounts of superplasticizer

Figure 2.2 shows the effect of alumina content on the rheological behavior of the suspensions. As expected, shear thinning behavior increased with alumina content since the coagulation of particles became more probable at higher levels of loading [15].

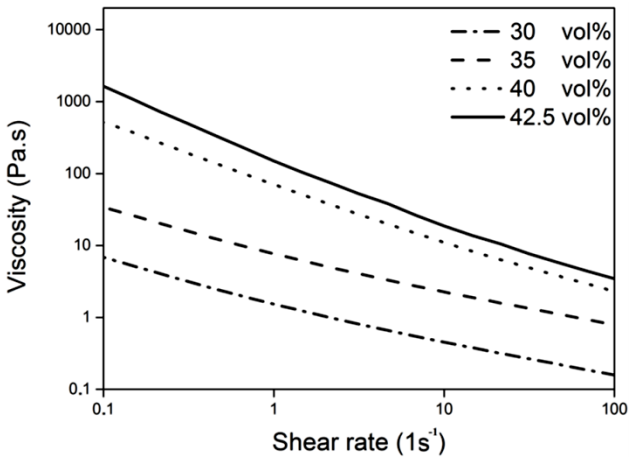

Figure 2.2 Viscosity of alumina suspensions as a function of shear rate in the presence of 1.25 wt. % superplasticizer

Krieger-Dougherty model is used to determine maximum particle loading in suspensions [16]:

$$\mu = \mu_0 (1 - {}^{\phi}/_{\phi_{max}})^{-(\frac{\mu}{\phi max})} \quad (1)$$

Where μ is the viscosity of the suspension (Pa.s), μ_0 is the viscosity of the media (Pa.s), ϕ_{max} is the maximum particle loading (vol. %) achievable for a system. Feeding particle loadings and viscosities to Krieger and Dougherty model at 1 s^{-1} shear rate provided a ϕ_{max} value of 45.7 vol. % that agrees well with the ϕ_{max} obtained from the results of extensional rheology (chapter 1).

2. 3 Mechanical characterization and machinability of green bodies

Traditionally, binders such as poly(vinyl alcohol), poly(ethylene imine), poly(vinyl pyrrolidone), and high molecular weight poly(ethylene glycol) were used to increase the mechanical strength of the green bodies that are slip cast from suspensions [17, 18]. These binders are usually employed at least more than 4 wt. % and although adding more binder contributes to the mechanical properties, it hinders the flowability of the slurry during casting [19]. Rheology modifiers such as poly(acrylic acid), poly(maleic acid), and Na-carboxymethyl cellulose were utilized in the presence of binders to homogenize the slurries and impose better packing of particles. In these systems, total amount of additive can reach to 4–10 wt. % [20]. Even at these concentrations of the polymers, machinable green bodies were not reported. On the other hand, in gel casting process, a common method to produce

machinable green bodies, crosslinkable polymers (e.g., poly(acrylamide) and poly(ethylene glycol) dimethacrylate) are used to form a network to host ceramic particles [21]. In these systems, the polymer content is 10–15 wt. %. In all of these methods, there is a need for careful binder burnout procedure, which can be as slow as 1 °C/min, to prevent structural defects that may appear due to the presence of the polymers at aforementioned amounts [22, 23]. Here, the compression tests were performed on 30–40 vol. % alumina loaded samples with 1.25 wt. % superplasticizer without any binders. The packing of the green bodies were tracked with helium pycnometry to find their percentage theoretical density. As expected, the compressive strength and percentage theoretical density of green bodies increased with alumina loading (Figure 2.3). The percentage of theoretical density at 30 vol. % loading was larger than 55 vol. % loaded gel cast samples that were previously reported [24, 25].

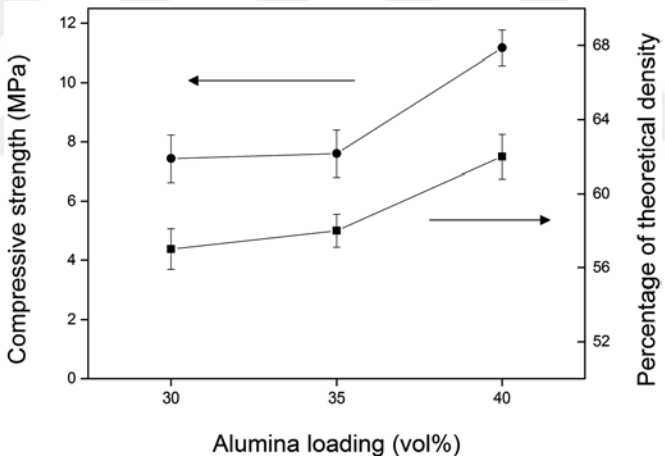

Figure 2.3 Compressive strength and percentage of theoretical density of green bodies with different vol. % alumina loadings at 1.25 wt. % superplasticizer addition

Although, it is desirable to have high strength green bodies, fifteen samples with 40 vol. % alumina content could not withstand machining and failed during the process. Therefore, a concentration of 35 vol. % alumina (with 1.25 wt. % superplasticizer) was chosen for testing reliability of green body machining. We consistently get smooth surfaces without visible cracks (over 60 samples) as exemplified by the inset in Figure 2.4a and b. The largest inner diameter of 8.2 mm was attained with a wall thickness of ~1.25 mm indicating that the green body can go through 59 % volume reduction (inset in Fig. 2.4a) without any crack formation. Sintered solid cast bodies shrunk 16.2 ± 1.8 % at the outer

diameter and 17.5 ± 0.9 % at the inner diameter independent of the initial diameter of the drill bit. Figure 2.4b exemplifies a lathed green body before sintering; this terraced body had a smooth surface and did not experience any cracking during the process. Machined green bodies fabricated by solid casting were similar to those which were produced via gel casting, starch consolidation, and protein coagulation casting in terms of green body strength and reproducibility [26-28].

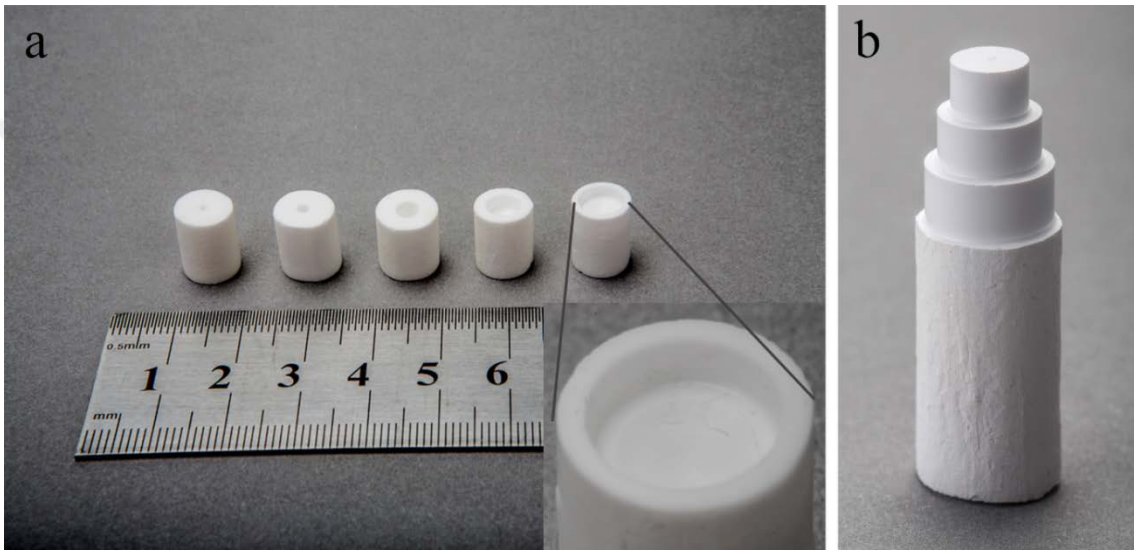

Figure 2.4 Photograph of a) sintered alumina samples that were drilled with (from left to right) 1.1, 2, 4, 6, and 8.2 mm drill bits before sintering, b) a green body after lathing

2.4 Conclusion

Here, by the use of a single additive, a PCE-based superplasticizer, we demonstrated the machinability of solid cast green bodies. This superplasticizer provided sufficient mechanical strength such that green bodies could withstand machining operations with no visible cracks and flaws. Exclusion of binders from the green body eliminated the time-consuming binder burnout step. We believe that the use of this superplasticizer can also be extended to other types of solid cast ceramics.

2.5 Reference

[1] E.M. Rabinovich, S. Leitner, A. Golden Berg, Slip casting of silicon nitride for pressureless sintering, Journal of Materials Science, 17 (1982) 323-328.
[2] C. Tallon, M. Limacher, G.V. Franks, Effect of particle size on the shaping of ceramics by slip casting, Journal of the European Ceramic Society, 30 (2010) 2819-2826.

[3] M.H. Talou, A.G.T. Martinez, M.A. Camerucci, Green mechanical evaluation of mullite porous compacts prepared by pre-gelling starch consolidation, Materials Science and Engineering: A, 549 (2012) 30-37.
[4] Y.-H. Koh, J.W. Halloran, Green Machining of a Thermoplastic Ceramic-Ethylene Ethyl Acrylate/Isobutyl Methacrylate Compound, Journal of the American Ceramic Society, 87 (2004) 1575-1577.
[5] R.K. Kamboj, S. Dhara, P. Bhargava, Machining behaviour of green gelcast ceramics, Journal of the European Ceramic Society, 23 (2003) 1005-1011.
[6] R. Janssen, S. Scheppokat, N. Claussen, Tailor-made ceramic-based components—Advantages by reactive processing and advanced shaping techniques, Journal of the European Ceramic Society, 28 (2008) 1369-1379.
[7] K.M. Lindqvist, E. Carlström, Indirect solid freeform fabrication by binder assisted slip casting, Journal of the European Ceramic Society, 25 (2005) 3539-3545.
[8] M. Li, P. Gehre, C.G. Aneziris, Investigation of calcium zirconate ceramic synthesized by slip casting and calcination, Journal of the European Ceramic Society, 33 (2013) 2007-2012.
[9] R.G. Neves, B. Ferrari, A.J. Sanchez-Herencia, C. Pagnoux, E. Gordo, Role of stabilisers in the design of Ti aqueous suspensions for pressure slip casting, Powder Technology, 263 (2014) 81-88.
[10] S. Mohanty, A.P. Rameshbabu, S. Mandal, B. Su, S. Dhara, Critical issues in near net shape forming via green machining of ceramics: A case study of alumina dental crown, Journal of Asian Ceramic Societies, 1 (2013) 274-281.
[11] S. Leo, C. Tallon, G.V. Franks, Aqueous and Nonaqueous Colloidal Processing of Difficult-to-Densify Ceramics: Suspension Rheology and Particle Packing, Journal of the American Ceramic Society, 97 (2014) 3807-3817.
[12] H. Bouhamed, S. Boufi, A. Magnin, Alumina interaction with AMPS–MPEG copolymers produced by RAFT polymerization: Stability and rheological behavior, Journal of Colloid and Interface Science, 333 (2009) 209-220.
[13] B. Jiang, S. Zhou, H. Ji, B. Liao, H. Pang, Dispersion and rheological properties of ceramic suspensions using linear polyacrylate copolymers with carboxylic groups as superplasticizer, Colloids and Surfaces A: Physicochemical and Engineering Aspects, 396 (2012) 310-316.
[14] S. Mohanty, B. Das, S. Dhara, Poly(maleic acid) – A novel dispersant for aqueous alumina slurry, Journal of Asian Ceramic Societies, 1 (2013) 184-190.
[15] B. Loebbecke, R. Knitter, J. Haußelt, Rheological properties of alumina feedstocks for the low-pressure injection moulding process, Journal of the European Ceramic Society, 29 (2009) 1595-1602.
[16] I.M. Krieger, T.J. Dougherty, A Mechanism for Non-Newtonian Flow in Suspensions of Rigid Spheres, Transactions of the Society of Rheology, 3 (1959) 137-152.
[17] A.-L. Kjøniksen, B. Nyström, Effects of Polymer Concentration and Cross-Linking Density on Rheology of Chemically Cross-Linked Poly(vinyl alcohol) near the Gelation Threshold, Macromolecules, 29 (1996) 5215-5222.
[18] M. Acosta, V.L. Wiesner, C.J. Martinez, R.W. Trice, J.P. Youngblood, Effect of Polyvinylpyrrolidone Additions on the Rheology of Aqueous, Highly Loaded Alumina Suspensions, Journal of the American Ceramic Society, 96 (2013) 1372-1382.
[19] X. Li, Q. Li, YAG ceramic processed by slip casting via aqueous slurries, Ceramics International, 34 (2008) 397-401.

[20] A.M. Kjeldsen, R.J. Flatt, L. Bergström, Relating the molecular structure of comb-type superplasticizers to the compression rheology of MgO suspensions, Cement and Concrete Research, 36 (2006) 1231-1239.
[21] J. Yu, J. Yang, Y. Huang, The transformation mechanism from suspension to green body and the development of colloidal forming, Ceramics International, 37 (2011) 1435-1451.
[22] J. Yang, J. Yu, Y. Huang, Recent developments in gelcasting of ceramics, Journal of the European Ceramic Society, 31 (2011) 2569-2591.
[23] X. Mao, S. Shimai, M. Dong, S. Wang, Gelcasting of Alumina Using Epoxy Resin as a Gelling Agent, Journal of the American Ceramic Society, 90 (2007) 986-988.
[24] K. Prabhakaran, C. Pavithran, Gelcasting of alumina from acidic aqueous medium using acrylic acid, Journal of the European Ceramic Society, 20 (2000) 1115-1119.
[25] K. Cai, Y. Huang, J. Yang, Alumina gelcasting by using HEMA system, Journal of the European Ceramic Society, 25 (2005) 1089-1093.
[26] S.H. Ng, J.B. Hull, J.L. Henshall, Machining of novel alumina/cyanoacrylate green ceramic compacts, Journal of Materials Processing Technology, 175 (2006) 299-305.
[27] J. Chandradass, K.H. Kim, D.s. Bae, K. Prasad, G. Balachandar, S.A. Divya, M. Balasubramanian, Starch consolidation of alumina: Fabrication and mechanical properties, Journal of the European Ceramic Society, 29 (2009) 2219-2224.
[28] B. Su, S. Dhara, L. Wang, Green ceramic machining: A top-down approach for the rapid fabrication of complex-shaped ceramics, Journal of the European Ceramic Society, 28 (2008) 2109-2115.

Chapter 3 Poly(carboxylate ether)-based superplasticizer achieves workability retention in calcium aluminate cement

This chapter is written based on the article "Poly(carboxylate ether)-based superplasticizer achives workability retention in calcium aluminate cement". Here, we report a modified superplasticizer that caters to the properties of Calcium aluminate cement (CAC) such as high rate of surface development and surface charge. While neat CAC was almost unworkable after 1 hour, with the addition of only 0.4 % of the optimized superplasticizer, 90 % fluidity retention was achieved.

3.1 Introduction

CAC is the cement of choice for high performance applications such as those requiring resistance to abrasion, corrosion, and temperature [1-3]. Due to its high early heat and strength gain, CAC has also become an attractive binder for cold environments and situations that necessitate rapid repairs (e.g., highways, bridge decks, and airport runways). In general, long term durability of cementitious mixtures requires low water/cement ratio (w/c). At low water contents, superplasticizers, which are polymers that can facilitate the dispersion of cement particles, are utilized to provide necessary workability. Superplasticizers adsorb onto the surface of the cement particles through their charged backbone and provide electrostatic repulsion [4, 5]. They release the entrapped water from flocculated structures and modify the viscosity of cement mixtures [6, 7]. Latest generations, poly(carboxylate ether)-based superplasticizers, (PCEs), have acrylate groups in the backbone and also contain side chains (i.e., poly(ethylene oxide)) that protrude from the cement surface into the pore solution to produce steric hindrance effect [8, 9]. These grafted polymers exhibit superior dispersing ability compared to other types of superplasticizers (e.g., melamine and naphthalene based polycondensates) and are efficient in the preparation of high performance concrete [5, 10, 11].

The formulations of PCEs have always targeted ordinary Portland cement (OPC) since it is the most frequently used binder in cement industry. However, these superplasticizers are incompatible with CAC due to i) the rapid hydration reaction of monocalcium aluminate as the principal active phase in this type of cement, and ii) layered

structure of hydration phases in CAC compared to amorphous calcium-silicate-hydrate (C-S-H) in OPC [6, 12, 13]. The use of PCEs in CAC systems resulted in poor fluidity retention (~15 min) and intercalation/sequestration of PCEs into lamellar calcium aluminate hydrates [13, 14]. Due to the absence of CAC-optimized superplasticizer, CAC systems are utilized in their neat form and consequently lose their workability in a relatively short amount of time [15]. Therefore, for wider and more efficient use of CAC, there is a need for the design of superplasticizers that can accommodate the characteristic properties of CAC.

To incorporate into the acrylic acid (AA) backbone of PCEs, we have chosen two co-monomers, 2-acrylamido-2-methylpropane sulfonic acid (AMPS) and vinylphosphonic acid (VPA), with different i) ionic character and ii) ability of association with multivalent cations. AMPS exhibits strong ionic character [16] whereas VPA demonstrates strong complexation ability with divalent cations [17, 18]. To comprehend the criteria of adsorption and workability retention, we cross-compared the performance of superplasticizers that contain varying amounts of AMPS and VPA in both OPC and CAC systems. The effect of both co-monomers on electrokinetic behavior of cement suspensions and rheological response of cement pastes were explored to design a dedicated superplasticizer for CAC. The fast reaction kinetics of hydrating CAC can be accommodated by controlled adsorption of VPA-modified PCEs (VPA-PCEs) that leads to the workability retention of the cement paste for longer periods of time (> 1 hour). This type of PCEs is the first set of superplasticizers to enable fluidity retention of CAC systems.

Eight PCEs with increasing amounts of modifying co-monomer in the backbone, referred to as X5, X10, X20, and X30 (X: VPA, AMPS) were prepared [19]. Figure 3.1a and b shows H^1-NMR of PCEs.

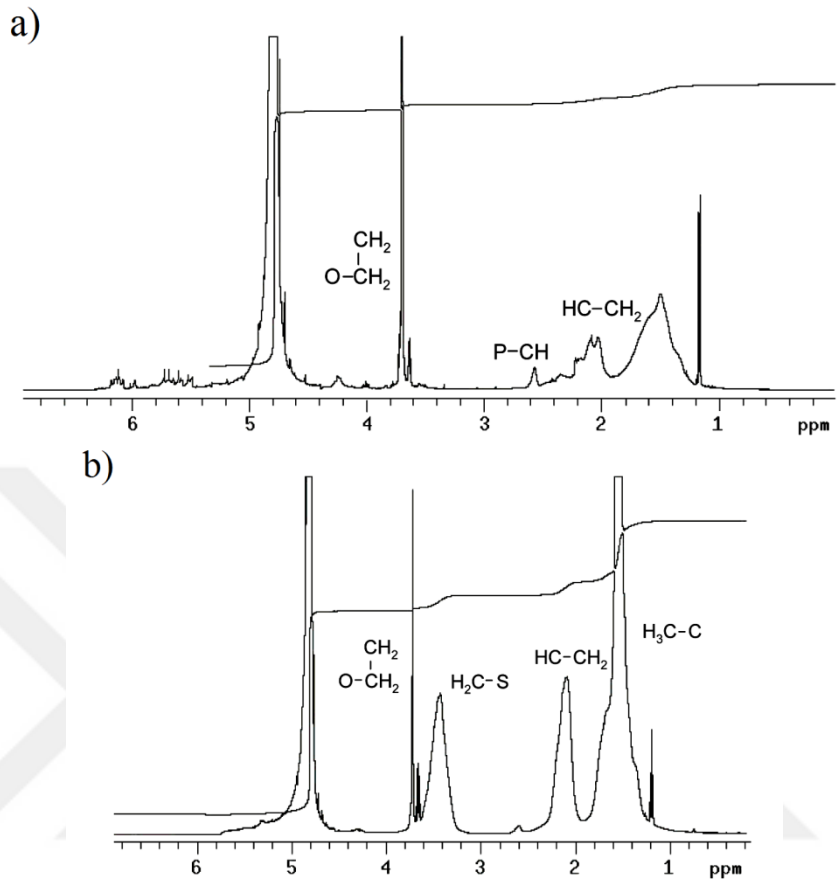

Figure 3.1 Representative H^1-NMR of PCEs: a) VPA20 and b) AMPS30

Molar ratios of building blocks and characteristic properties of PCEs were shown in Table 3.1. Charge density and Ca-complexion ability of superplasticizers were calculated from direct addition of NaOH and $Ca(OH)_2$ to polymer solution by titration, respectively.

Table 3.1 Molar composition and characteristic properties of PCEs

	Molar feed ratio	Sample acronym	$\frac{\text{VPA}}{\text{AA}}$	$\frac{\text{PEG}}{\text{AA + VPA}}$	$\frac{\text{mmol anionic site}}{\text{1 mg solid}}$	$\frac{\text{mmol bound Ca}}{\text{1 mg solid}}$
VPA/AA/PEG	5/45/1	VPA 5	0.8/10	1.1/100	4.1×10^{-3}	3.7×10^{-3}
	10/40/1	VPA 10	1.6/10	0.9/100	4.2×10^{-3}	3.9×10^{-3}
	20/30/1	VPA 20	3.4/10	1/100	4.4×10^{-3}	4.0×10^{-3}
	30/20/1	VPA 30	5.6/10	0.7/100	5.2×10^{-3}	4.2×10^{-3}
	Molar feed ratio	Sample acronym	$\frac{\text{AMPS}}{\text{AA}}$	$\frac{\text{PEG}}{\text{AA + AMPS}}$		
AMPS/AA/PEG	5/45/1	AMPS 5	3.1/10	0.6/100	4.6×10^{-3}	3.6×10^{-3}
	10/40/1	AMPS 10	4.2/10	0.5/100	5.6×10^{-3}	2.9×10^{-3}
	20/30/1	AMPS 20	7.5/10	0.5/100	5.8×10^{-3}	2.1×10^{-3}
	30/20/1	AMPS 30	17/10	0.7/100	6.2×10^{-3}	1.4×10^{-3}

All of the copolymers contain PEG-1000 side chains with a density of less than 1.1 %. The general chemical structure of superplasticizers was shown in Figure 3.2.

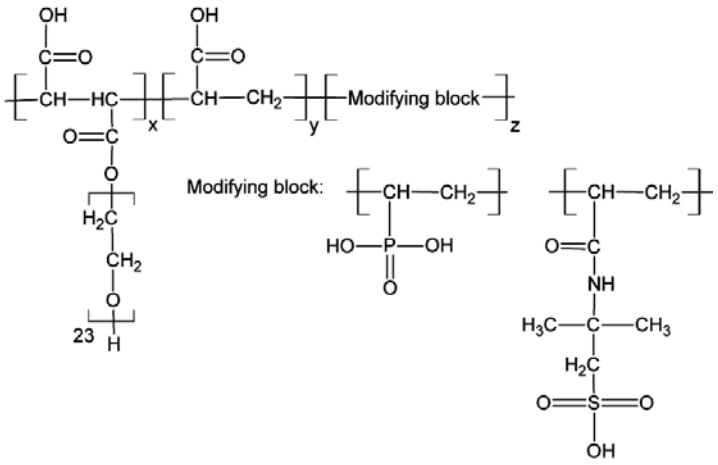

Figure 3.2 General chemical structure of superplasticizers

3.1 Adsorption behavior and electro-kinetic study

The dispersing ability of PCEs depends on the adsorption of the copolymer onto the cement particles. Adsorption of PCEs typically follows the Langmuir monolayer model

while multi-layer adsorption is plausible at high dosages of PCEs [20-22]. We first tracked the adsorption of modified-PCEs through measuring the amount of unadsorbed copolymer that remains in the solution (depletion method) [10]. Once adsorption starts, the amount of adsorbed PCEs in AMPS-PCEs/OPC, VPA-PCEs/OPC, and VPA-PCEs/CAC systems increases linearly with the amount of added polymer at low dosages (Figure 3.3). The adsorption, then, stabilizes to a plateau value (i.e., adsorption saturation) confirming the Langmuir monolayer adsorption behavior of PCEs in these systems. This plateau indicates complete coverage of cement particles by PCEs while the slope of the linear range is related to the affinity of PCEs to the cement particles [14]. VPA-PCEs exhibited lower adsorption tendency compared to AMPS-PCEs in both OPC and CAC systems; whereas utilization of anionic co-monomer (AMPS-PCEs) caused depletion of the PCEs from CAC suspensions. To elucidate the effect of modifying block on induced charge of the cement particles upon adsorption of PCEs, zeta potentials were evaluated at differing amounts of polymer in the cement suspension. In general, interactions of PCEs and cement particles comprise i) the electrostatic interactions and ii) formation of complexes between the Ca^{2+} and the ionic backbone of PCEs [21, 23]. Unlike direct electrostatic adsorption of PCEs, adsorption through Ca^{2+} bridging has little influence on the zeta potential of cement particles [22]. AMPS co-monomer adsorbs onto the surface of the cement particles through strong conjugation in its sulfonate group (SO^{3-}) [24]. Compared to carboxylic group of AA, which is a weak acid with strong complexation ability, sulfonic group is a stronger acid and mainly interacts with the surface of the cement particles via electrostatic interactions [25]. Lower basicity of the oxyanion in SO^{3-} compared to that of acrylate (COO^{-}) reduces the charge transfer to counterions and results in ionic character of its bonding with counterions [24]. On the other hand, phosphonate groups (PO_3^{2-}) present more basic oxyanions than COO^{-} and its bi-functionality, compared to mono-negative charge of COO^{-}, gives rise to strong complexation with multivalent cations [17, 18]. Therefore, substitution of AA with AMPS co-monomer encourages the shift of surface potentials to higher negative values whereas VPA substitution is expected to impart a slight change on the surface charge of the particles.

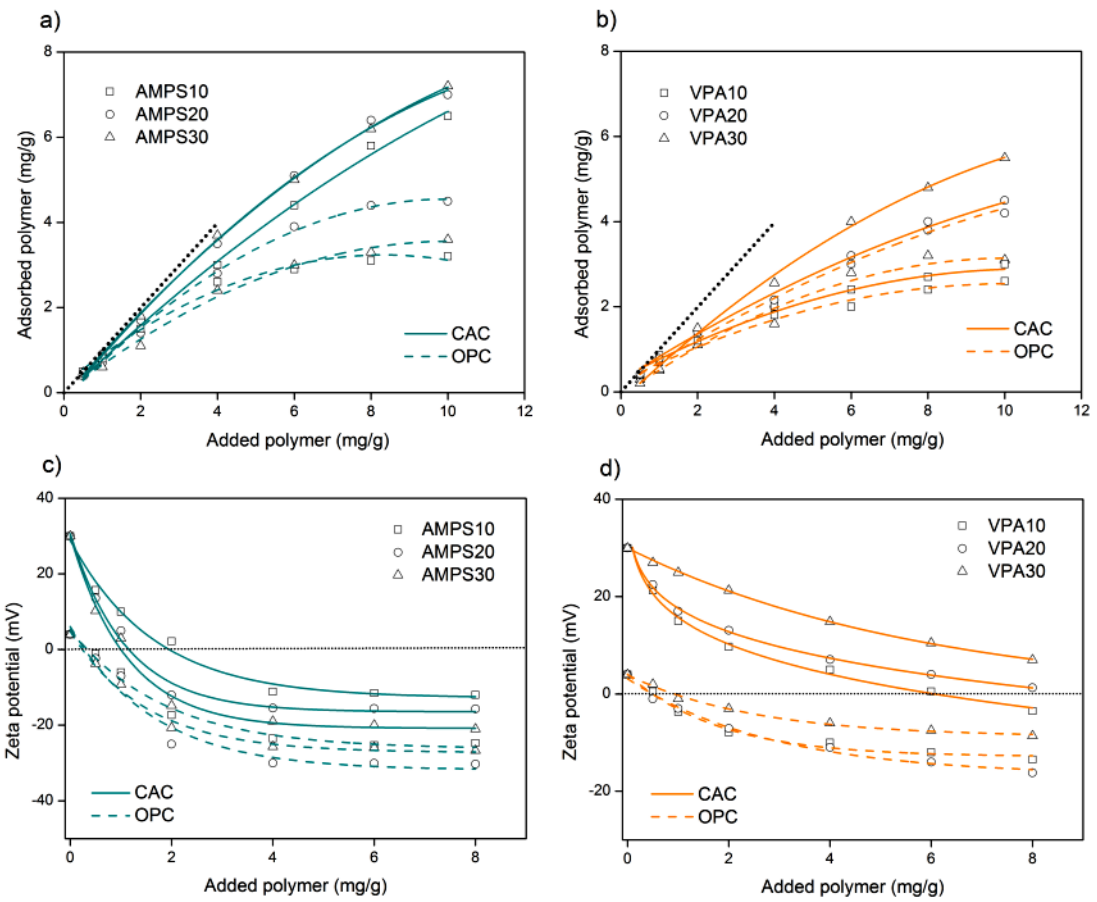

Figure 3.3 Adsorption behavior of (a) AMPS-PCEs and (b) VPA-PCEs on the surface of cement particles as a function of polymer dosage (dotted lines show 100 % adsorption). Zeta potential of cement suspensions in the presence of (c) AMPS-PCEs and (d) VPA-PCEs

In hydrating OPC, the presence of negatively charged silicate and positively charged aluminate phases leads to the formation of heterogeneous charge distribution on the surface of particles [26]. Compared to OPC, CAC, whose main component is monocalcium aluminate, offers higher positive zeta potential and thus, more anchorage points for direct adsorption due to the fast reaction of the aluminate phase at early stages of hydration [3]. Upon adsorption, zeta potential of suspensions decreased from +4 mV in neat OPC and from +30 mV in neat CAC (Figure 3.3c and d) confirming that negatively charged PCEs progressively consume positive charges on the surface of the particles. PCEs, once adsorbed, bring more negative charges to the surface than needed to compensate all of the positive ones. Therefore, increasing amount of adsorbed PCEs eventually leads to an inversion of the zeta potential (overcharging effect) [27]. In OPC systems, the decrease in

zeta potential ceases at 6–8 mg/g of PCEs that is consistent with the dosages where the particles are fully covered (Figure 3.3a and b). After full coverage of OPC particles with AMPS-PCEs, overcharging effect is clearly observed where zeta potential lowers below -20 mV. However, in CAC, surface of particles offers more positively charged areas; thus, it is less susceptible to overcharging effect. As a result, inversion of zeta potential appears at higher dosages and zeta potential cannot go below -15 ± 4 mV in CAC systems.

To further understand the role of surface charge density on instability of CAC suspensions, surface area of the neat cement in the first 5 minutes of hydration (during mixing process) was determined (Figure 3.4).

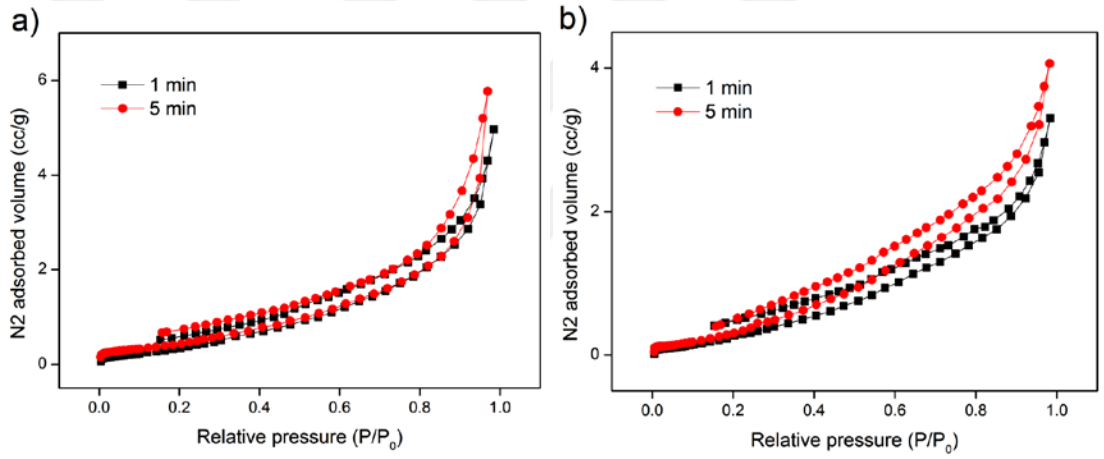

Figure 3.4 N2 adsorption-desorption isotherm of a) OPC and b) CAC with hydration time

In early stages of CAC hydration, unequal solubility of Ca^{2+} and aluminate ions leads to roughening of the surface and enrichment of Al_2O_3. This incongruent solubility of ions increases the surface area and charge density of the hydrating particles, whereby double hydroxides of cationic $[Ca_2Al(OH)_6]^+$ are formed as the hydrating product [28, 29]. In agreement with the results of Mangabhai [29], we have also observed high rate of surface development in CAC suspensions (Table 3.2) that is accompanied by the introduction of high positive potentials to the surface of particles (+30 mV). Therefore, high rate of surface development, surface charge density of hydrating particles, and affinity of adsorption result in depletion of anionic PCEs (AMPS-PCEs) from CAC suspensions.

Table 3.2 BET surface area of hydrating cement

	BET surface area (m^2/g)		
	1 min hydration	3 min hydration	5 min hydration
Neat OPC	1.5	1.8	2.1
Neat CAC	1.8	2.1	2.3

In VPA-PCEs/CAC systems, the highest amount of phosphonate substitution (VPA30) resulted in i) the least overcharging effect (i.e., no inversion in the sign of zeta potential) and ii) the highest Ca^{2+} complexation as demonstrated by Ca^{2+} titration and conductivity measurements (Figure 3.5). In agreement with the less ionic character of phosphonate group compared to that of carboxylate group, these observations illustrate that Ca^{2+} mediated adsorption is the dominant process for VPA-PCEs/CAC systems. Therefore, through the utilization of phosphonic groups, adsorption affinity of PCEs to the surface of CAC particles is lowered and the change of surface potential is restrained upon adsorption.

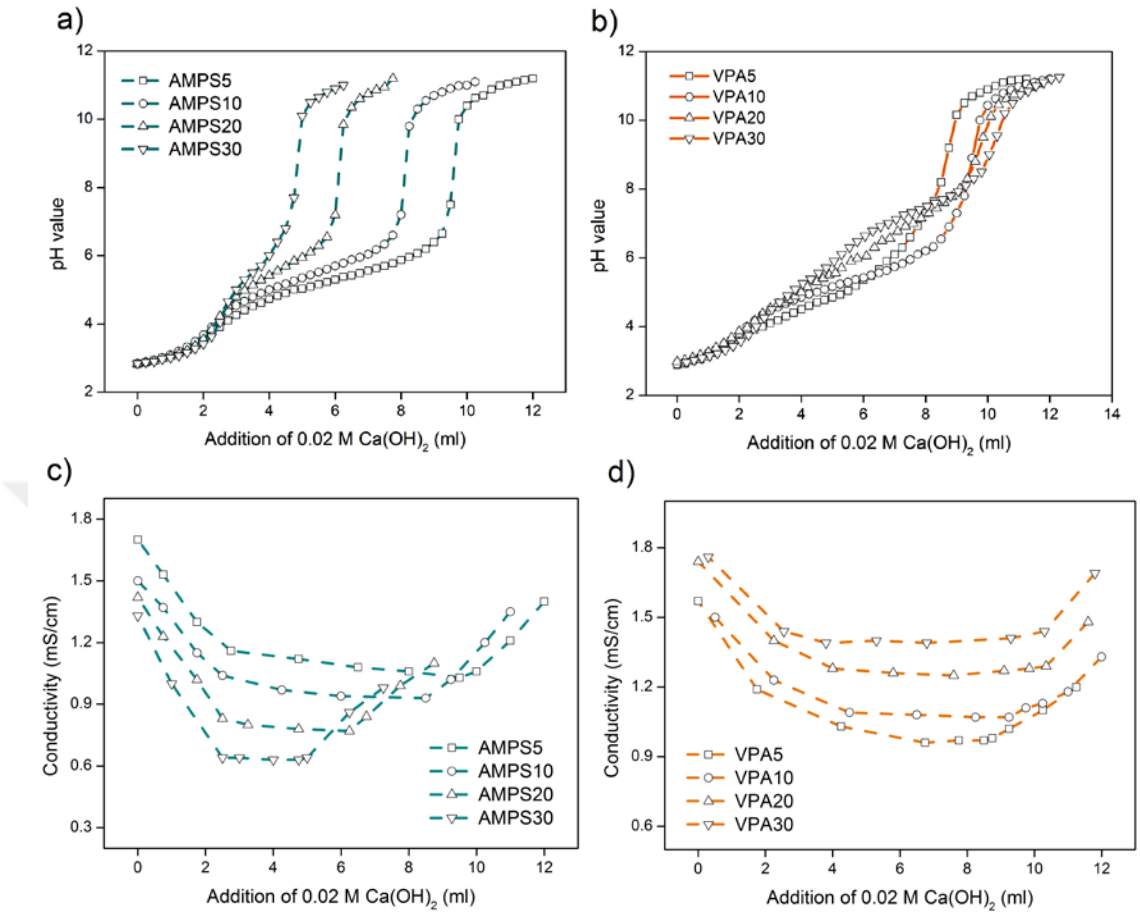

Figure 3.5 Ca-titration (a and b) and conductivity measurements (c and d) of PCEs

3.2. Flow behavior and workability retention of cement pastes

Flow behavior of cement pastes depends on the physical and chemical interactions among its components: cement particles, admixtures (e.g., superplasticizers and stabilizing agents), and water [12]. Generally, the adsorption of superplasticizers on cement particles deflocculates the aggregate structure of the fresh paste and releases the restrained water and therefore, gives rise to an improved fluidity of cement mixtures [30]. To assess the compatibility of superplasticizers and cement, we carried out a mini slump test as a function of dosage of PCEs [31]. In this test, a cone of a height of 60 mm, and bottom and top diameter of 40 mm and 20 mm, respectively, is filled with cement paste and spread diameter is recorded after pulling out the cone. Typically, the flow diameter of cement mixtures increases with low concentration of the superplasticizers, and then, reaches a plateau at a certain dosage (i.e., critical dosage). Beyond this critical dosage, fluidity of the mixture does not depend on the amount of superplasticizer since the dispersion state of

particles does not change with further addition of the superplasticizer [21]. On the other hand, incomplete surface coverage of particles below a “minimum dosage” might decrease fluidity of the mixtures due to inhomogeneity in charge distribution and broad range of surface potentials [31]. Critical and minimum dosages were tracked to understand the effect of ionicity of the polymers on the fluidity of cement pastes. In AMPS-PCEs/OPC systems, as the content of AMPS is increased in the backbone, the minimum dosage shifted from 0.6 % by weight of cement (hereafter wt. %) in AMPS5 to 0.1 wt. % in AMPS30, and the critical dosage changed from 0.8 wt. % in AMPS5 to 0.4 wt. % in AMPS30 (Figure 3.6).

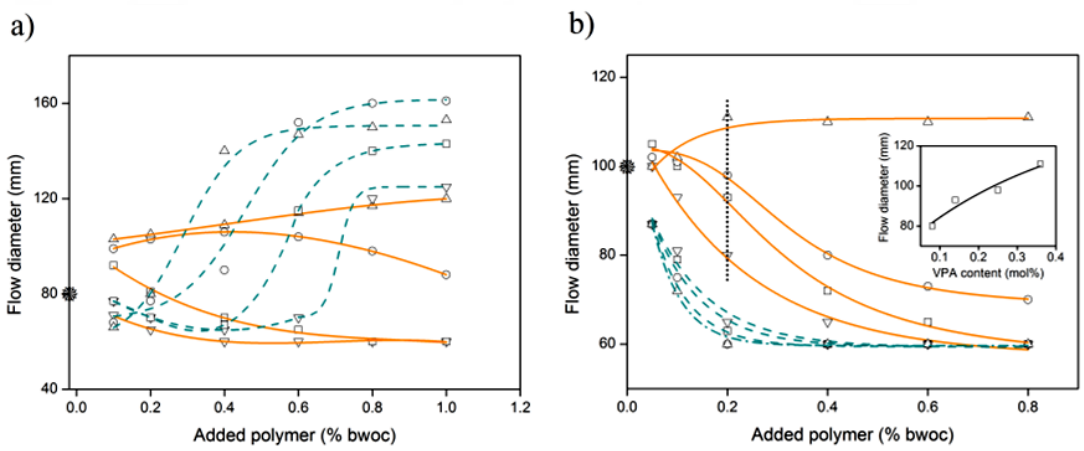

Figure 3.6 Fluidity behavior of (a) OPC and (b) CAC pastes in the presence of AMPS-PCEs (dash-line) and VPA-PCEs (solid line), (∇): X5, (□): X10, (○): X20, and (Δ): X30. Solid star shows flow diameter of neat cement pastes. Inset of figure 2b shows flow diameter of CAC pastes in the presence of 0.2 % VPA-PCEs as a function of VPA content in the backbone of copolymer

Moreover, minimum dosages overlap with the dosages that surface potentials of particles enter into the electrostatically stable region (< -20 mV, Figure 3.3c) and particles experience homogeneous charge distribution (Figure 3.7).

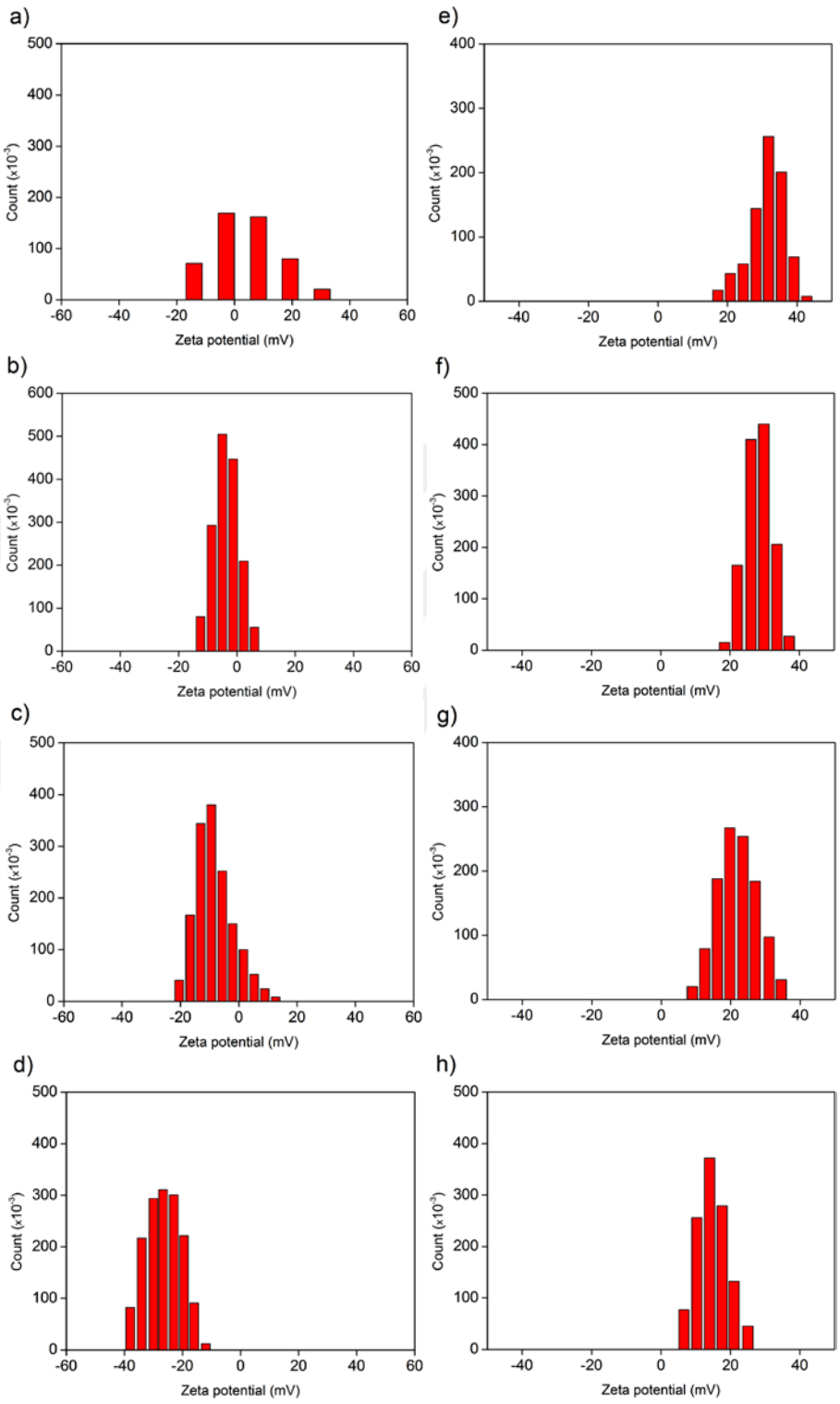

Figure 3.7 Zeta potential distribution of OPC-AMPS30 mixtures with PCEs content of a) 0 wt. %, b) 0.05 wt. %, c) 0.1 wt. %, d) 0.2 wt. %, and CAC-VPA30 mixtures with PCEs content of e) 0 wt. %, f) 0.05 wt. %, g) 0.2 wt. %, and h) 0.4 wt. %

Concurrently, critical dosages coincide with the beginning of the plateau region where surface of particles are fully covered by PCEs (Figure 3.3a and c). With rise of AMPS content of PCEs, the flow diameter of mixtures at critical dosages has increased to 120–150 mm compared to flow diameter of 80 ± 3 mm in neat OPC paste. Observed correlation between fluidity of OPC pastes and magnitude of zeta potentials in AMPS-PCEs/OPC systems indicates that electrostatic repulsion capacity of the PCEs plays a key role in dispersability of these anionic superplasticizers [32, 33]. In VPA-PCEs/OPC systems, due to reduced affinity of adsorption and lower ionicity of VPA compared to AMPS, adsorption of VPA-PCEs cannot impart enough charge onto OPC particles (Figure 3.3d). Lower fluidity of VPA-PCEs/OPC systems compared to that of AMPS-PCEs/OPC confirms that PCEs with higher anionic character are more favored for OPC paste for enhanced fluidity and compatibility.

In AMPS-PCEs/CAC systems, the flow diameter of cement paste is decreased at all dosages (Figure 3.3b) such that increasing ionicity of the AMPS-PCEs progressively lowers the fluidity of the pastes. As shown in Figure 3.8, destabilization and quick setting of CAC paste underscores the incompatibility of CAC and a PCE-based copolymer with high anionic character.

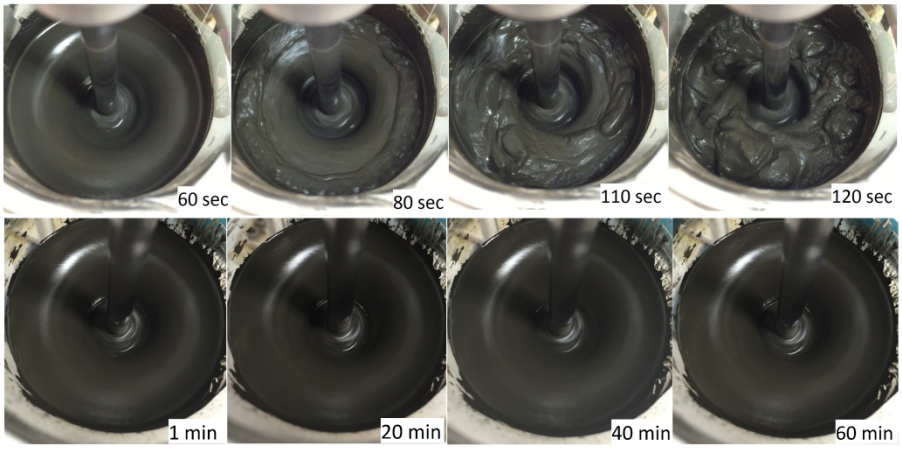

Figure 3.8 Top: quick setting of CAC paste in the presence of 0.5 % AMPS30 and bottom: fluidity of CAC paste in the presence of 0.5 % VPA30

This incompatibility originates from high rate of surface development (Table 3.2) and high surface charge density of CAC particles (Figure 3.3c) that rapidly deplete AMPS-

PCEs from the pore solution (Figure 3.3a). It is important to note that zeta potentials of larger than 20 mV (or smaller than -20 mV) are typically preferred for stable suspensions [34, 35]. Hence, AMPS-PCEs whose dispersing ability mostly relies on electrostatic interactions cannot form stable CAC suspensions even after full coverage of the particles. On the other hand, reduction of ionicity of PCEs by incorporation of VPA into the backbone progressively improves the fluidity of CAC pastes (dotted line in Figure 3.6b) and led to observation of a critical dosage at 0.2 wt. % of superplasticizer in VPA30. Enhanced compatibility of CAC with VPA30 (Figure 3) underlines that adsorption of PCEs through electrostatic interactions are detrimental for fluidity of CAC pastes. On the other hand, utilization of co-monomers with strong complexation ability facilitates the dispersion of CAC particles. In these systems, the fluidity behavior of the paste does not follow the zeta potential but rather directly correlates with the amount of adsorbed superplasticizer. Therefore, steric repulsion dominates the deflocculation of the dispersion [36-38].

The dispersion state of CAC particles in the presence of VPA30 and AMPS30 is also tracked by measuring the average particle size (d_{ave}) and particle size distribution (PDI) of CAC suspensions (Figure 3.9).

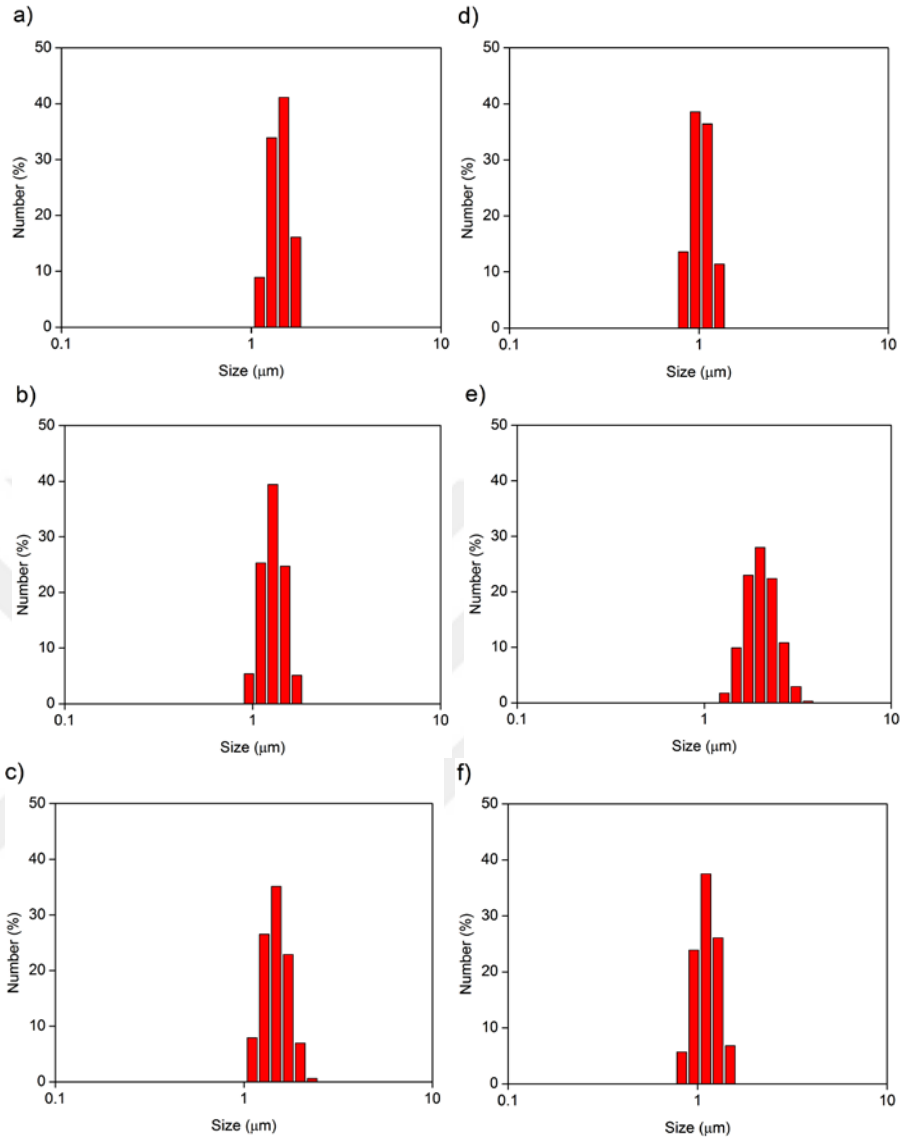

Figure 3.9 Size distribution of cement particles with and without 0.5 wt. % PCEs: a) neat OPC, (b) OPC-AMPS30, c) OPC-VPA30, d) neat CAC, e) CAC-AMPS30, and f) CAC-VPA30

In the presence of VPA30, d_{avg} and PDI decreased slightly illustrating colloidal stability of the system whereas the size of flocs increased from 3.9 ± 0.5 μm in neat CAC suspension to 6.3 ± 1.3 μm in the presence of AMPS30 (Figure 3.10, Table 3.3).

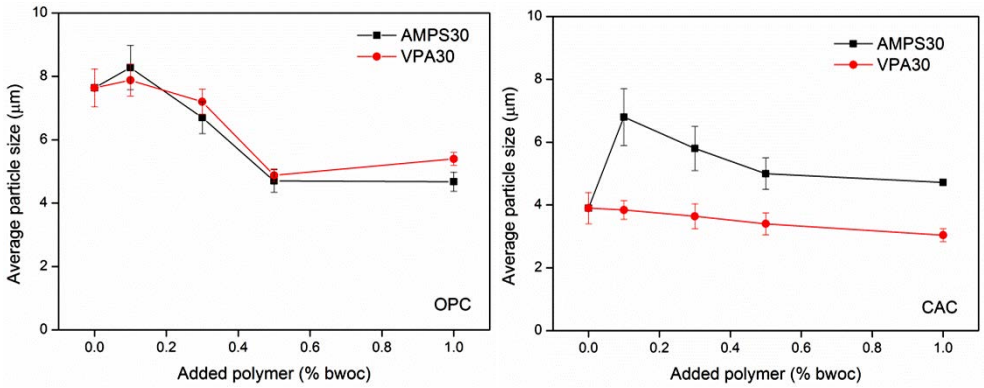

Figure 3.10 Effects of PCEs on the average particle size of OPC and CAC suspension

This increase in floc size demonstrates the formation of assembled structures (Figure 3.8) and hence, higher amount of entrapped water in flocculated particles [21].

Table 3.3 Polydispersity index of suspensions with and without 0.5 wt. % PCEs

	OPC system	CAC system
Neat cement	0.80±0.1	0.53±0.02
AMPS-30	0.33±0.05	0.78±0.1
VPA-30	0.45±0.1	0.58±0.05

To quantitatively evaluate the effect of modifying co-monomers and thus, dispersion state of particles on the fluidity of mixtures, rheological measurements were carried out on cement pastes. By fitting the experimental points of descending part of shear rate-shear stress curve (Figure 3.11) with Bingham equation ($\tau = \tau_0 + \eta\dot{\gamma}$), two parameters are tracked; i) yield stress (τ_0, Pa) as a measure of the shear stress required to initiate flow and ii) plastic viscosity (η, Pa.s) as a measure of material resistance to flow after the initiation of the flow [39]. While yield stress is proportional to the particle–particle interactions in cement mixtures; plastic viscosity relates to the size of the flocs and varies with particle size distribution in cement particles [40, 41].

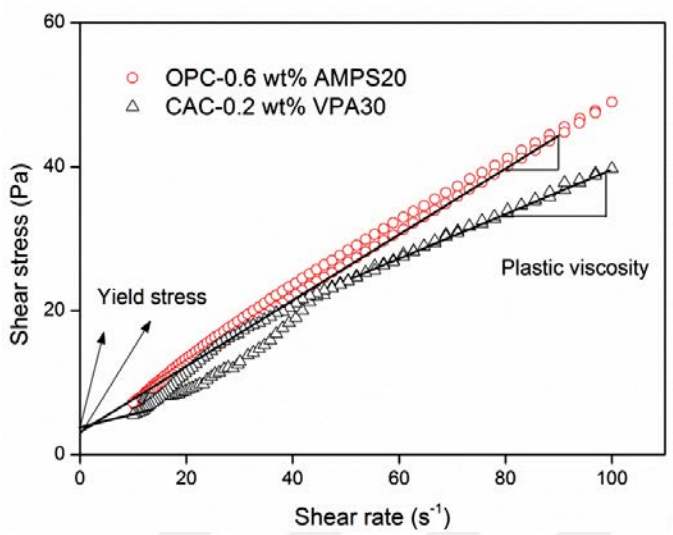

Figure 3.11 Hysteresis cycles with illustration of yield stress and plastic viscosity for cement pastes with admixtures

Compared to neat CAC paste, VPA30 reduced the yield stress more than 35 % (Table 3.4 and 5). Introduction of AMPS to PCEs progressively reduces the yield stress and plastic viscosity of OPC pastes such that more than 80 % reduction of yield stress was measured in the saturation dosage of AMPS30. This pronounced effect of anionic PCEs is fully linked with higher dispersing ability of these PCEs and narrow size distribution of flocs in OPC paste. However, this increasing ionicity has an adverse effect on CAC suspensions such that rheological parameters of CAC pastes could not be assessed as all of the AMPS-PCEs/CAC pastes showed severe coagulation upon addition of these anionic superplasticizers.

Table 3.4 Yield stress and plastic viscosity for OPC pastes and admixture dosage (n.d.: not determined due to severe flocculation)

	Dosage of PCEs (% bwoc)	Yield stress (Pa)	Plastic viscosity (Pa.s)
Pure OPC		14.4 ±1	0.5
AMPS10	0.2	10.1±0.5	0.58
	0.4	n.d.	n.d.
	0.6	n.d.	n.d.
AMPS20	0.2	7.7±0.4	0.90
	0.4	5.9±0.4	0.80
	0.6	5±0.2	0.67
AMPS30	0.2	14.2±1	0.49
	0.4	2.5±0.6	0.30
	0.6	2.1±0.5	0.35
VPA10	0.1	13±0.5	0.47
	0.2	14±0.7	0.58
	0.4	n.d.	n.d.
VPA20	0.1	13±0.3	0.41
	0.2	12±0.2	0.40
	0.4	11±0.2	0.39
VPA30	0.1	13.5±0.3	0.41
	0.2	12±0.3	0.41
	0.4	10.4±0.2	0.39

Table 3.5 Yield stress and plastic viscosity for CAC pastes and admixture dosage (n.d.: not determined)

	Dosage of PCEs (% bwoc)	Yield stress (Pa)	Plastic viscosity (Pa.s)
Pure CAC		7.8±0.3	0.30
VPA10	0.1	9.5±0.4	0.45
	0.2	11.1±0.5	0.41
	0.4	n.d.	n.d.
VPA20	0.1	7.5±0.3	0.36
	0.2	8.9±0.4	0.38
	0.4	14±0.5	0.40
VPA30	0.1	6.5±0.3	0.44
	0.2	5±0.2	0.46
	0.4	4.6±0.2	0.45

Increase of anionicity of PCEs has been shown to enhance the adsorption rate of superplasticizers onto OPC particles and hence, initial workability of the system [42]. However, retaining this induced fluidity depends on the gradual adsorption of PCEs from the pore solution [43, 44]. OPC, which has lower surface charge compared to CAC, can sustain gradual adsorption of the copolymer. On the other hand, anionic copolymers (AMPS-PCEs) got immediately adsorbed onto the CAC particles due to high surface development and charge in CAC systems. This depletion of AMPS-PCEs from the pore solution reduces the dispersing ability of this set of superplasticizers [13]. Therefore, achieving high initial fluidity and workability retention in CAC necessitates a controlled adsorption onto the particles. To evaluate the time dependent workability (fluidity retention behavior) of cement pastes, superplasticizers with the highest dispersing ability in each system were chosen and fluidity of the system was measured with varying dosages of the PCEs over a period of 60 min (Figure 3.12).

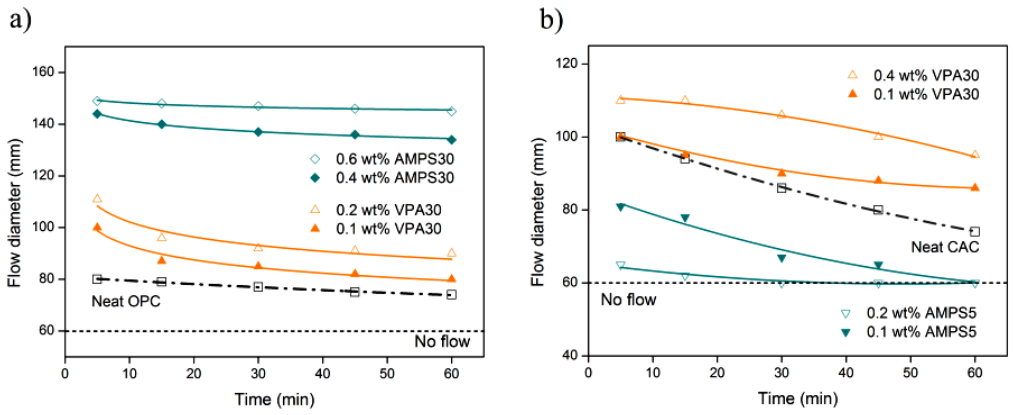

Figure 3.12 Time dependent fluidity of a) OPC and b) CAC pastes in the presence of PCEs with highest dispersing ability

After addition of VPA30 to CAC and OPC pastes, fluidity retention in both systems was clearly improved. In VPA30-CAC system that contains 0.4 wt. % superplasticizer, only a 9 % decrease in flow diameter was observed after 60 min. In the absence of PCEs, both CAC and OPC showed ~ 50 % reduction in flowability after 60 min while approaching to the line of "no flow" at a diameter of 60 mm.

3.3 Conclusion

In widely used OPC systems, high affinity between the superplasticizer and the cement particles provides fluidity and stable dispersions. However, in CAC systems, gradual adsorption is necessary in order to avoid depletion of the superplasticizer from the suspension and accommodate the high surface charge and increasing surface area of the hydrating CAC particles. We utilized a co-monomer with less ionic character but with strong complexation ability, VPA, to offer controlled adsorption of PCEs and for the first time in literature, demonstrated workability retention of CAC pastes compared to the neat CAC systems. We believe this result will potentially open up venues for wider and more efficient use of calcium aluminate cement.

3.4 Reference

[1] N. Ukrainczyk, T. Matusinović, Thermal properties of hydrating calcium aluminate cement pastes, Cement and Concrete Research, 40 (2010) 128-136.
[2] N. Ukrainczyk, Kinetic modeling of calcium aluminate cement hydration, Chemical Engineering Science, 65 (2010) 5605-5614.

[3] E. Sakai, T. Sugiyama, T. Saito, M. Daimon, Mechanical properties and micro-structures of calcium aluminate based ultra high strength cement, Cement and Concrete Research, 40 (2010) 966-970.
[4] A. Habbaba, A. Lange, J. Plank, Synthesis and performance of a modified polycarboxylate dispersant for concrete possessing enhanced cement compatibility, Journal of Applied Polymer Science, 129 (2013) 346-353.
[5] G. Duan, G. Huang, A. Li, Y. Zhu, Y. Gong, A study of supermolecular polarization of comb-like polycarboxylate admixtures synthesized with polyoxyethylene macromolecules, Journal of Molecular Liquids, 174 (2012) 129-134.
[6] K.L. Scrivener, J.-L. Cabiron, R. Letourneux, High-performance concretes from calcium aluminate cements, Cement and Concrete Research, 29 (1999) 1215-1223.
[7] G. Falzone, M. Balonis, G. Sant, X-AFm stabilization as a mechanism of bypassing conversion phenomena in calcium aluminate cements, Cement and Concrete Research, 72 (2015) 54-68.
[8] W. Fan, F. Stoffelbach, J. Rieger, L. Regnaud, A. Vichot, B. Bresson, N. Lequeux, A new class of organosilane-modified polycarboxylate superplasticizers with low sulfate sensitivity, Cement and Concrete Research, 42 (2012) 166-172.
[9] T.-S. Liao, C.-L. Hwang, Y.-S. Ye, K.-C. Hsu, Effects of a carboxylic acid/sulfonic acid copolymer on the material properties of cementitious materials, Cement and Concrete Research, 36 (2006) 650-655.
[10] X. Liu, Z. Wang, J. Zhu, Y. Zheng, S. Cui, M. Lan, H. Li, Synthesis, characterization and performance of a polycarboxylate superplasticizer with amide structure, Colloids and Surfaces A: Physicochemical and Engineering Aspects, 448 (2014) 119-129.
[11] A. Büyükyağcı, G. Tuzcu, L. Aras, Synthesis of copolymers of methoxy polyethylene glycol acrylate and 2-acrylamido-2-methyl-1-propanesulfonic acid: Its characterization and application as superplasticizer in concrete, Cement and Concrete Research, 39 (2009) 629-635.
[12] O. Burgos-Montes, M. Palacios, P. Rivilla, F. Puertas, Compatibility between superplasticizer admixtures and cements with mineral additions, Construction and Building Materials, 31 (2012) 300-309.
[13] S. Ng, E. Metwalli, P. Müller-Buschbaum, J. Plank, Occurrence of intercalation of PCE superplasticizers in calcium aluminate cement under actual application conditions, as evidenced by SAXS analysis, Cement and Concrete Research, 54 (2013) 191-198.
[14] M.d.M. Alonso, M. Palacios, F. Puertas, Effect of Polycarboxylate–Ether Admixtures on Calcium Aluminate Cement Pastes. Part 1: Compatibility Studies, Industrial & Engineering Chemistry Research, 52 (2013) 17323-17329.
[15] V.G.P.B. H. Fryda, K. Scrivener, Interaction of Superplasticizers with Calcium Aluminate Cements, Special Publication, 195.
[16] Y.-R. Zhang, X.-M. Kong, Z.-B. Lu, Z.-C. Lu, S.-S. Hou, Effects of the charge characteristics of polycarboxylate superplasticizers on the adsorption and the retardation in cement pastes, Cement and Concrete Research, 67 (2015) 184-196.
[17] J.H. Jones, Amino Acids and Peptides, Royal Society of Chemistry, 1992.
[18] L. Macarie, G. Ilia, Poly(vinylphosphonic acid) and its derivatives, Progress in Polymer Science, 35 (2010) 1078-1092.
[19] O. Akhlaghi, O. Akbulut, Y.Z. Menceloglu, Extensional rheology and stability behavior of alumina suspensions in the presence of AMPS-modified polycarboxylate ether-based copolymers, Colloid and Polymer Science, 293 (2015) 2867-2876.

[20] H.B. Bey, J. Hot, R. Baumann, N. Roussel, Consequences of competitive adsorption between polymers on the rheological behaviour of cement pastes, Cement and Concrete Composites, 54 (2014) 17-20.
[21] Y. Zhang, X. Kong, Correlations of the dispersing capability of NSF and PCE types of superplasticizer and their impacts on cement hydration with the adsorption in fresh cement pastes, Cement and Concrete Research, 69 (2015) 1-9.
[22] K. Yoshioka, E.-i. Tazawa, K. Kawai, T. Enohata, Adsorption characteristics of superplasticizers on cement component minerals, Cement and Concrete Research, 32 (2002) 1507-1513.
[23] T. Sowoidnich, T. Rachowski, C. Rößler, A. Völkel, H.-M. Ludwig, Calcium complexation and cluster formation as principal modes of action of polymers used as superplasticizer in cement systems, Cement and Concrete Research, 73 (2015) 42-50.
[24] K. Naka, H. Cölfen, K. Naka, T. Okamura, A. Onoda, K. Takahashi, N. Ueyama, H. Yamamoto, S.H. Yu, Biomineralization II: Mineralization Using Synthetic Polymers and Templates, Springer Berlin Heidelberg, 2006.
[25] B.L. Rivas, E. Pereira, A. Maureira, Functional water-soluble polymers: polymer–metal ion removal and biocide properties, Polymer International, 58 (2009) 1093-1114.
[26] J. Plank, M. Gretz, Study on the interaction between anionic and cationic latex particles and Portland cement, Colloids and Surfaces A: Physicochemical and Engineering Aspects, 330 (2008) 227-233.
[27] H. Bouhamed, S. Boufi, A. Magnin, Dispersion of alumina suspension using comb-like and diblock copolymers produced by RAFT polymerization of AMPS and MPEG, Journal of Colloid and Interface Science, 312 (2007) 279-291.
[28] C. Giraudeau, J.-B. D'Espinose De Lacaillerie, Z. Souguir, A. Nonat, R.J. Flatt, Surface and Intercalation Chemistry of Polycarboxylate Copolymers in Cementitious Systems, Journal of the American Ceramic Society, 92 (2009) 2471-2488.
[29] R.J. Mangabhai, Calcium Aluminate Cements: Proceedings of a Symposium dedicated to H G Midgley, London, July 1990, Taylor & Francis, 1990.
[30] E. Sakai, T. Kasuga, T. Sugiyama, K. Asaga, M. Daimon, Influence of superplasticizers on the hydration of cement and the pore structure of hardened cement, Cement and Concrete Research, 36 (2006) 2049-2053.
[31] R.J. Flatt, Towards a prediction of superplasticized concrete rheology, Materials and Structures, 37 (2004) 289-300.
[32] Y. Li, C. Yang, Y. Zhang, J. Zheng, H. Guo, M. Lu, Study on dispersion, adsorption and flow retaining behaviors of cement mortars with TPEG-type polyether kind polycarboxylate superplasticizers, Construction and Building Materials, 64 (2014) 324-332.
[33] M. Yang, C.M. Neubauer, H.M. Jennings, Interparticle potential and sedimentation behavior of cement suspensions, Advanced Cement Based Materials, 5 (1997) 1-7.
[34] F. Massazza, U. Costa, A. Barrila, Interaction Between Superplasticizers and Calcium Aluminate Hydrates, Journal of the American Ceramic Society, 65 (1982) 203-207.
[35] C.M. Neubauer, M. Yang, H.M. Jennings, Interparticle Potential and Sedimentation Behavior of Cement Suspensions: Effects of Admixtures, Advanced Cement Based Materials, 8 (1998) 17-27.
[36] H. Uchikawa, S. Hanehara, D. Sawaki, The role of steric repulsive force in the dispersion of cement particles in fresh paste prepared with organic admixture, Cement and Concrete Research, 27 (1997) 37-50.

[37] C.-Z. Li, N.-Q. Feng, Y.-D. Li, R.-J. Chen, Effects of polyethlene oxide chains on the performance of polycarboxylate-type water-reducers, Cement and Concrete Research, 35 (2005) 867-873.
[38] C. Schröfl, M. Gruber, J. Plank, Preferential adsorption of polycarboxylate superplasticizers on cement and silica fume in ultra-high performance concrete (UHPC), Cement and Concrete Research, 42 (2012) 1401-1408.
[39] S.E. Chidiac, F. Mahmoodzadeh, Plastic viscosity of fresh concrete – A critical review of predictions methods, Cement and Concrete Composites, 31 (2009) 535-544.
[40] M.M. Alonso, M. Palacios, F. Puertas, Compatibility between polycarboxylate-based admixtures and blended-cement pastes, Cement and Concrete Composites, 35 (2013) 151-162.
[41] Y. Tan, J. Ouyang, Y. Li, Factors influencing rheological properties of fresh cement asphalt emulsion paste, Construction and Building Materials, 68 (2014) 611-617.
[42] B. Felekoğlu, H. Sarıkahya, Effect of chemical structure of polycarboxylate-based superplasticizers on workability retention of self-compacting concrete, Construction and Building Materials, 22 (2008) 1972-1980.
[43] T.M. Vickers Jr, S.A. Farrington, J.R. Bury, L.E. Brower, Influence of dispersant structure and mixing speed on concrete slump retention, Cement and Concrete Research, 35 (2005) 1882-1890.
[44] R.J. Flatt, Y.F. Houst, A simplified view on chemical effects perturbing the action of superplasticizers, Cement and Concrete Research, 31 (2001) 1169-1176.

Chapter 4 Modified poly(carboxylate ether)-based superplasticizer for enhanced flowability of calcined clay-limestone-gypsum blended Portland cement

This chapter is written based on the article "Modified poly(carboxylate ether)-based superplasticizer for enhanced flowability of calcined clay-limestone-gypsum blended Portland cement". Here, we report the performance of a series of a modified poly(carboxylate ether)-based superplasticizers (PCEs) in a ternary ordinary Portland cement-calcined clay-limestone blend. The optimized polymer does not intercalate into the layered structure of calcined clay and preserves its steric size in the presence of high concentration of sulfate ions.

4.1 Introduction

Ordinary Portland cement (OPC) is the most produced human-made material and its production is responsible for approximately 8 % of total anthropogenic CO_2 emissions [1]. Materials with lower emissions, such as pozzolans, clays, fly ash, blast-furnace slag, and silica fume, are suggested to replace OPC [2-6]. However, this replacement is often associated with reduction of strength at early ages. Recently, introduction of limestone to these blends have been reported to remedy this problem through improving the reactivity of the system [7, 8]. Scrivener et al. [9, 10] and Habert et al. [11] have shown that the substitution of OPC, up to 50 %, with a combination of calcined clay, limestone, and gypsum offers an energy/cost-effective solution along with mechanical properties that are comparable to plain cement.

The utilization of supplementary materials has significant impact on fluidity of blended cement and thereby, an increase in water to binder ratio (w/b) is required to maintain necessary fluidity of these mixtures [12]. Similar to plain cement, high range water reducer agents, known as superplasticizers, are added to these blends to limit the amount of mixing water while retaining the workability at low w/b ratios. Latest generation of superplasticizers, PCEs, which exhibit superior dispersing ability compared to other types of superplasticizers (e.g., sulfonated naphthalene formaldehyde and sulfonated melamine formaldehyde) have acrylate groups in the backbone and contain polyethylene glycol (PEG) side chains that protrude from the cement surface into the pore solution [13-

15]. Despite the superior performance of PCEs in forming workable mixtures, their interaction with clay minerals and sulfate ions (SO_4^{2-}) still leads to a loss in fluidity or a higher water demand to achieve the same levels of workability of plain cement [15-17]. Based on the specific properties of clay minerals (e.g., layered structure and swelling ability), different type of clays can potentially increase the dosage of PCEs due to consumption of superplasticizers through intercalation. Therefore, highly-substituted mixtures require advanced superplasticizers that can address the high surface area and layered structure of the incorporated clay minerals as well as high concentration of sulfate ions in the pore solution.

4.2 Characterization of superplasticizers and materials proportioning

All copolymers, hereafter AMPS-PCEs, were synthesized by aqueous free radical polymerization of acrylic acid (AA), 2-acrylamido-2-methylpropane sulfonic acid (AMPS), and esterified-PEG-1000 [18]. Chemical structure of AMPS-PCEs was shown in Figure 4.1.

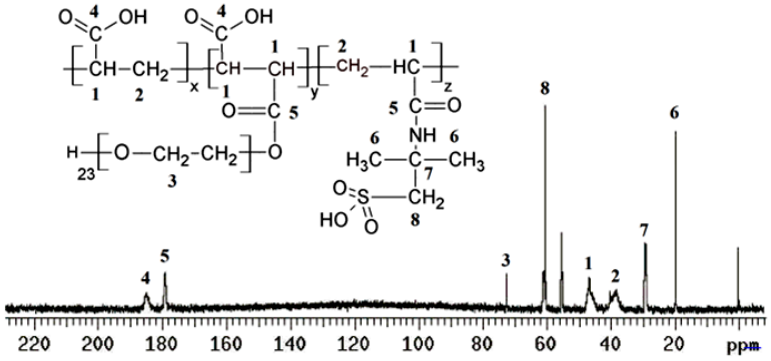

Figure 4.1 Representative C^{13}-NMR of AMPS-PCEs

Characteristic properties of the copolymers (quantitative H^1-NMR) were listed in Table 4.1. Charge density and Ca-complexion ability of AMPS-PCEs were calculated from direct addition of NaOH and $Ca(OH)_2$ to polymer solution by titration, respectively. Hydrodynamic radius of copolymers was measured from solution of 1 wt. % AMPS-PCEs in synthetic pore solution and intrinsic viscosity was evaluated by dilute solution viscometry (Cannon glass capillary viscometer 1C) at 22 °C.

Table 4.1 Molar composition and characteristic properties of studied AMPS-PCEs

	AMPS-PCE1	AMPS-PCE2	AMPS-PCE3
pH of synthesis	6	8	13
AMPS/AA	1.05/1	0.95/1	1/1
PEG/AMPS+AA	0.5/100	0.7/100	0.6/100
mmol anionic sites/mg solid	3.6×10^{-3}	3.6×10^{-3}	3.6×10^{-3}
mmol bound Ca/mg solid	1.8×10^{-3}	1.9×10^{-3}	1.9×10^{-3}
r_h (nm)	12 ± 1	10 ± 0.5	14 ± 1
Intrinsic viscosity (dl/g)	4.3	3.1	5.4
Mw (g/mol)	336,200	251,100	590,000
PDI (Mw/Mn)	2.89	2.72	3.63

Binders with different amounts of calcined clay, limestone, and gypsum were mixed with OPC to formulate binders of varying compositions (Table 4.2). Binder with 45 wt. % quartz substitutions was also prepared as control sample without addition of superplasticizer.

Table 4.2 Composition and nomenclature of the binders that are utilized in this work

Name of binder	OPC %	Calcined clay %	Limestone %	Gypsum %	Quartz %
OPC	100	0	0	0	0
C45	55	45	0	0	0
L5	55	40	5	0	0
L10	55	35	10	0	0
L15	55	30	15	0	0
G5	50	30	15	5	0
G3	55	28	14	3	0
G1.5	55	29	14.5	1.5	0
Q45	55	0	0	0	45

4.3 Fluidizing ability of AMPS-PCEs in plain OPC system

To optimize the performance of AMPS-PCEs in blended cement, we, first, assessed the fluidity behavior of OPC, as the main binder, in the presence of superplasticizers with varying chemical compositions and structures. Figure 4.2a shows the slump flow diameter of OPC pastes (w/c of 0.45) as a function of AMPS to AA ratio (AMPS/AA) in AMPS-PCEs. Increasing content of AMPS co-monomer improved the fluidity of the pastes up to AMPS/AA of 1 and beyond this point, the flow decreased towards the lowest slump diameter at AMPS/AA of 2.5. The improved fluidity also agrees well with the results of Liao et al. [19] that demonstrated the enhanced fluidity of OPC pastes through addition of linear copolymers of methacrylic acid and AMPS. To provide a relationship between density of PEG side chains (i.e., PEG/AA+AMPS mol/mol) and dispersing ability of copolymers, the performance of AMPS-PCEs with AA/AMPS of 1 but with varying side chain density was monitored in plain OPC pastes (Figure 4.2b). In these systems, side chain density of ≈ 0.7 % provided the highest fluidity as indicated by the highest spread diameters at all superplasticizer dosages. Therefore, AA/AMPS of 1 and side chain density of ≈ 0.7 % was chosen for further analysis. Superplasticizers with this chemical composition and structure but different molecular weight were then tested to fluidize the OPC and subsequently the blended cement pastes.

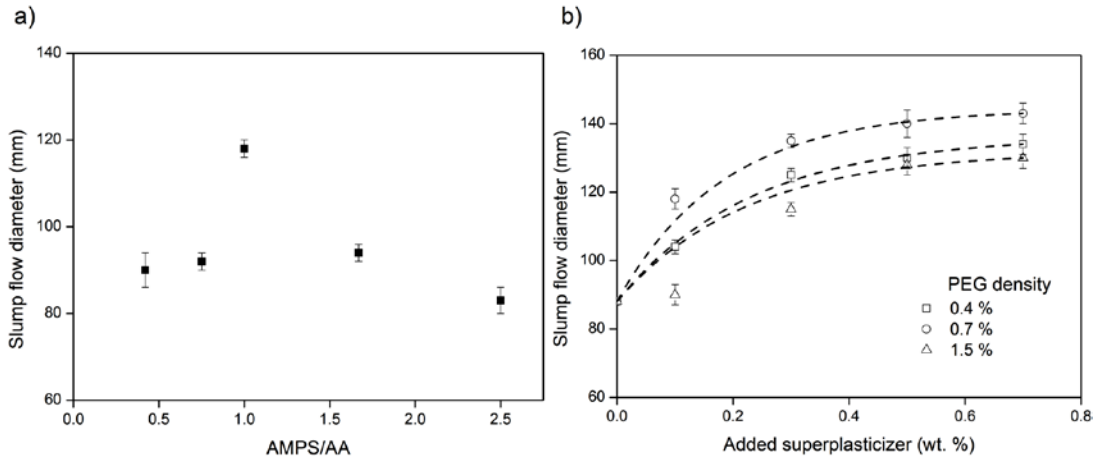

Figure 4.2 Effect of a) AMPS content (density of side chains was kept at ≈ 0.7 %, PCEs/cement = 0.1 wt. %) and b) density of grafted chains (AA/AMPS was kept at ≈1) on dispersing ability of AMPS-PCEs in OPC pastes

As shown in Figure 4.3a, utilization of AMPS-PCE2, which possesses the lowest molecular weight and hydrodynamic radius (Table 4.2), gave rise to better fluidity compared to AMPS-PCE1 and AMPS-PCE3 systems. The difference between dispersing ability of AMPS-PCE2 and other copolymers also became more pronounced at lower water content (w/c = 0.4). To characterize the effect of sulfate ions on performance of copolymers, slump flow test was also conducted at a high concentration of sulfate ions and low AMPS-PCEs/c of 0.1 wt. %. As shown in Figure 4.3b, spread diameter of OPC pastes decreased after addition of 0.2 mol/l sodium sulfate; however, among all polymers, AMPS-PCE2 induced the highest average flowability—only ~ 8% reduction.

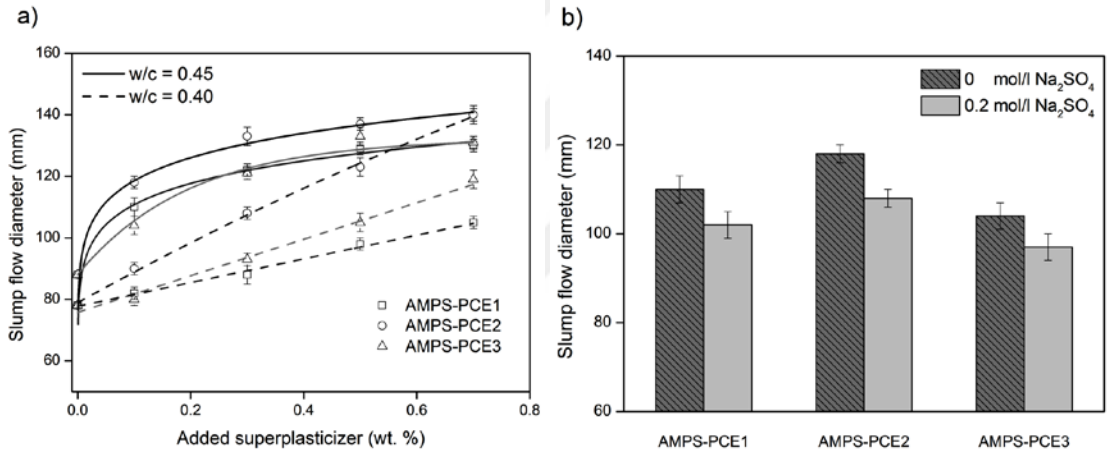

Figure 4.3 a) effect of molecular weight and amount of the copolymer on spread diameter of cement paste at different w/c, and b) slump flow diameter of OPC pastes with different PCEs at low and high concentration of sulfate ions (PCEs/c = 0.1 wt. %, w/c = 0.45)

4.4 Electro-kinetic study and adsorption behavior of AMPS-PCEs

In order to evaluate the dispersing ability of superplasticizers, variations in surface potential of particles were first measured in synthetic pore solution (Figure 4.4a–c). Upon adsorption of the superplasticizer, the zeta potentials of OPC, calcined clay, and limestone particles decreased from -11, -22, and -4.5 mV, respectively, reaching higher absolute values and leveling off at ~ 4–6 mg/g polymer addition. This gradual decrease in zeta potentials confirms that AMPS-PCEs bring more negative charge to the surface of particles than that is needed to compensate for the surface charges. AMPS-PCE2 offers the highest electrostatic interactions with binders that is evidenced by the most negative value of zeta

potential at the plateau region of the curves. This result is also in agreement with the higher charge density of AMPS-PCE2 compared to that of AMPS-PCE1 and AMPS-PCE3 (Table 4.1). Due to superior electro-kinetic properties of AMPS-PCE2, this copolymer performed better compared to other copolymers in inducing fluidity at i) low w/c and ii) in the presence of sulfate ions. Therefore, we have singled out this copolymer for further testing.

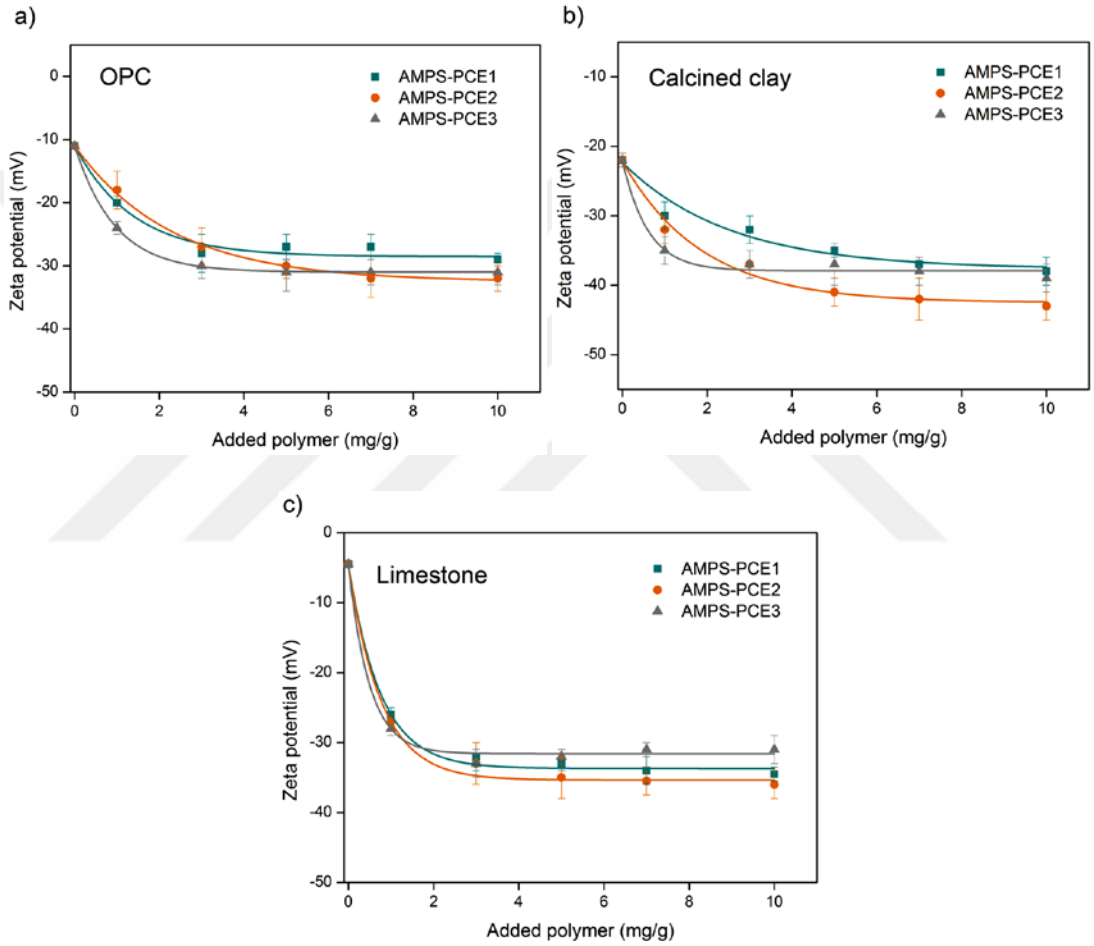

Figure 4.4 Zeta potential of a) OPC, b) clay, and c) limestone particles as a function of added AMPS-PCEs

Adsorption isotherm was performed as a function of superplasticizer content in the synthetic pore solution. As shown in Figure 4.5, the adsorption of the AMPS-PCE2 onto cement, calcined clay, and limestone particles follows a typical Langmuir monolayer adsorption model [20]; the amount of adsorption increases linearly at low dosages and then stabilizes near a plateau (i.e., adsorption saturation). While adsorption saturation indicates complete coverage of binder particles with superplasticizer, the slope of the linear range is

related to the affinity of superplasticizer to the particles [21]. This type of adsorption is consistent with previous reports on adsorption behavior of PCEs onto cement, limestone, and clay particles [22-26]. Considering the slope of the linear range of adsorption isotherms, AMPS-PCE2 exhibited the highest tendency of adsorption to limestone whereas a controlled adsorption was observed in OPC system. This higher tendency is also supported by a sudden drop in surface potential of limestone particles while that of OPC particles displayed a gradual decrease upon adsorption of the copolymer (Figure 4.4a and b). In addition, adsorption curves start to level off at 4–6 mg/g AMPS-PCEs/binder that is consistent with the dosages where zeta potential exhibits a plateau region, confirming the full coverage of particles by the copolymer molecules.

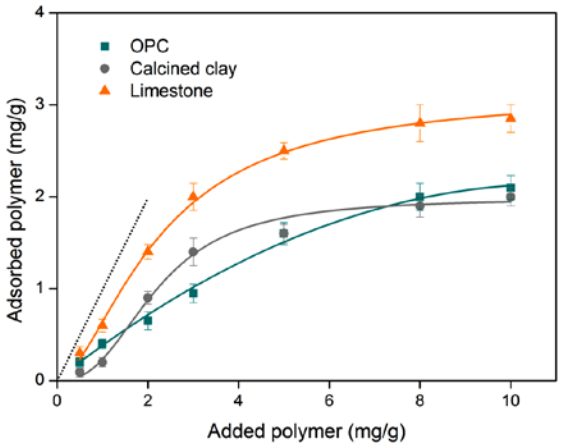

Figure 4.5 Adsorption behavior of AMPS-PCE2 on the surface of different particles in synthetic pore solution (dotted-line shows 100 % adsorption)

When cement grains are dispersed in aqueous medium, formation of different hydrate phases leads to the development of heterogeneous surface structure and thus, heterogeneous charge distribution on cement grains—silicate and aluminate hydrates exhibit negative and positive surface charge, respectively. In general, the adsorption of PCEs in cementitious systems comprises i) the direct electrostatic adsorption to positively charged phases and ii) indirect adsorption to negatively charged phases through bridging with Ca^{2+} in the pore solution (i.e., complexation) [27-29]. Formation of complexes between PCEs and Ca^{2+} is mainly influenced by the type of functional group in the backbone of the copolymer. Acrylic acid monomer has carboxylic group (COOH) in its structure, which is a weak acid with strong complexation ability. On the other hand, AMPS co-monomer contains sulfonic

group (SO_3H) as the interaction site, which is a strong acid, and mainly interacts with the particles through electrostatic forces [30, 31]. The strong conjugation of SO_3^- in this co-monomer lowers the basicity of the oxyanion and charge transfer to the counter ions. This lower basicity results in ionic character of the bonding and reduces the complexation ability of sulfonate compared to carboxylate group [32]. In order to comprehend the criteria of adsorption as well as copolymer-particle interaction, variations in zeta potential of particles were tracked as a function of AMPS-PCE2 dosage in water. As shown in Figure 4.6, OPC and limestone offer zeta potential values of +2 and +15 mV, respectively with notable change in surface potential upon the adsorption of the copolymer. On the other hand, calcined clay particles that exhibit zeta potential of -21 mV hardly interact with AMPS-PCE2 since electrostatic interaction does not favor the adsorption of the copolymer. Hence, it can be concluded that high amount of adsorption of the copolymer by OPC and limestone particles in the pore solution (Figure 4.5) is due to available sites for both direct adsorption and complexation, while interaction of AMPS-PCEs with clay particles mostly relies on the presence of multivalent cations (e.g., Ca^{2+}) in the medium to complex PCEs onto the surface of clay particles (Figure 6 compared to Figure 4b).

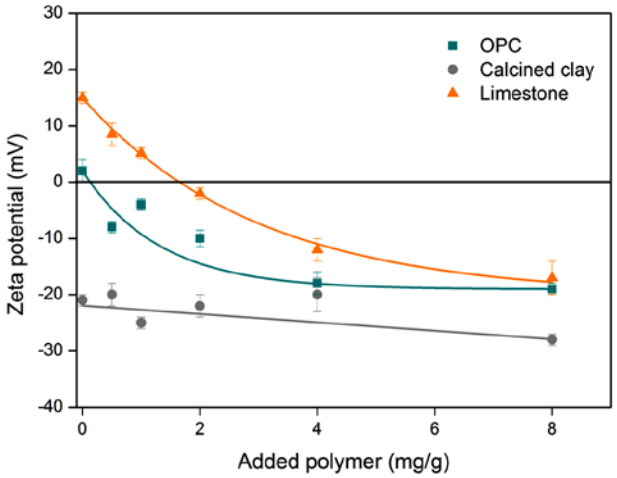

Figure 4.6 Zeta potential of binders as a function of AMPS-PCE2 in water

4.5 Fluidity behavior of blended cement

To assess the dispersing ability of AMPS-PCE2 in blended cement, mini slump test was carried out on pastes with various amounts of binders as a function of dosage of the copolymer. As shown in Figure 4.7a, incorporation of 45 wt. % calcined clay particles

(C45) to OPC requires addition of a “minimum dosage” of 0.3 wt. % AMPS-PCE2. Appearance of this minimum dosage is due to the increase in the specific surface area of blended cement compared to plain OPC [33]. Beyond the minimum dosage, the slump flow diameter increases towards the maximum fluidity at 1 wt. % while further addition of the superplasticizer slightly reduces the fluidity. In agreement with saturation dosage of components (Figure 4.5), this reduction is attributed to the excess amount of PCEs that can cause bridging flocculation [34]. Upon addition of limestone to blends, not only the minimum dosage raised to 0.5 wt. %, but also the overall fluidity was reduced with increasing content of limestone (L5, L10, and L15 in Figure 4.7a). Since limestone exhibits highest affinity of adsorption and also highest saturation dosage (Figure 4.5), the introduction of limestone into the binder mixtures results in consumption of the superplasticizer in the pore solution and thus, lower fluidity is expected. On the other hand, inclusion of 1.5 and 3 wt. % gypsum (G1.5 and G3 in Figure 4.7b) improved the initial slump flow diameter of the pastes—G1.5 > G3> L15. Similar increase in initial fluidity with the addition of gypsum was also reported by Okamura et al. [35] and attributed to depressed hydration of aluminate-containing phases.

To evaluate time dependent workability (fluidity retention) of pastes, we utilized 1 wt. % AMPS-PCE2 and fluidity retention tests were carried out over a period of 60 min. As shown in Figure 4.7c, no significant reduction was observed in slump diameter of mixtures containing calcined clay and limestone (C45, L5, L10, and L15) up to 60 min. On the other hand, addition of gypsum changed the slump retention behavior of pastes (G1.5 and G3)—higher percentage of gypsum led to higher slump loss over time. In order to understand the effect of gypsum on reaction kinetics, isothermal calorimetry was performed on OPC, G1.5, and G5 (Figure 4.7d, normalized with respect to the content of cement). In general, heat evolution in hydrating OPC comprises 4 stages; i) dissolution, ii) induction, iii) acceleration, and iv) deceleration periods [2, 36]. As seen in Figure 4.7d, the addition of 1 wt. % AMPS-PCE2 prolonged the induction period for all studied mixtures. This prolonged induction period can be attributed to the hindering effect of adsorbed copolymers on dissolution of silicate phases (i.e., retardation effect) [23]. However, this effect can be minimized in the case of blends with calcined clay-limestone-gypsum because the reaction takes place earlier. The reaction on the aluminates seems to be little influenced by the

addition of polymers but mainly controlled by the presence of gypsum (G5+PCEs compared to G1.5+PCEs in Figure 4.7d). It is then very likely that higher rate of slump loss, when gypsum is incorporated to the blends, is attributed to i) accelerated rate of hydration—increasing the cohesiveness of the blended cement, and ii) formation of sulfoaluminoferrite hydrates (e.g., ettringite) that preferentially adsorb PCEs and reduce the available superplasticizer in the pore solution [37].

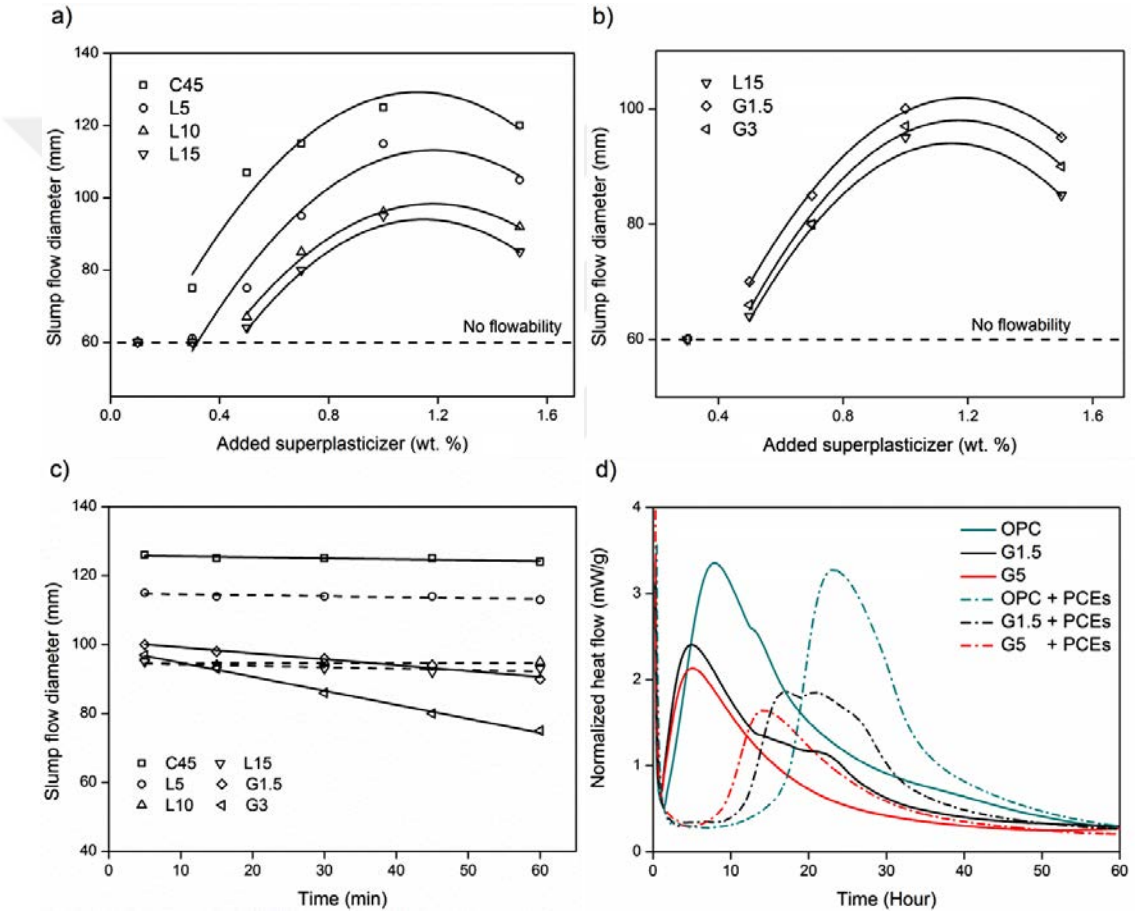

Figure 4.7 Effect of a) limestone and b) gypsum on flowability of blends with increasing AMPS-PCE2 content, c) effect of time on fluidity of blends containing 1 wt. % AMPS-PCE2, and d) isothermal calorimetric curves of OPC and blended systems with/without 1 wt. % AMPS-PCE2

Increase of anionicity of PCEs has been shown to enhance the adsorption rate of copolymers onto cementitious particles and hence, initial workability of the system. However, retaining this induced fluidity requires gradual adsorption of PCEs from the pore solution [38-40]. Furthermore, dispersing ability of these superplasticizers in OPC-calcined

clay-limestone-gypsum system is affected by layered structure of clay and presence of sulfate ions. The PEG side chains have been known to intercalate (i.e., chemisorb) into the aluminosilicate layers of clays. Instead of adsorbing onto the surface of cement, the superplasticizer is consumed by clay through chemisorption, and thus dispersing ability of the superplasticizer declines [16, 17]. Presence of sulfate ions can also lead to reduction of dispersing ability of PCEs via decreasing the steric size of superplasticizer and condensation of grafted chains. This sensitivity to sulfate ions originates from i) the competition between COO^- groups in the backbone of the copolymer and SO_4^{2-} in the pore solution for attaching to the surface of cement particles and ii) decrease in the repulsive force between ionized groups of the backbone that can lead to the shrinkage of the PCEs [15, 41]. In order to correlate the ability of AMPS-PCE2 to retain workability of blends, we monitored i) the amount of remaining copolymer in the pore solution of L15, ii) structural changes in calcined clay, and iii) steric size of AMPS-PCE2 in the presence of elevated concentration of sulfate ions. The content of AMPS-PCE2in the pore solution that initially includes 10 mg/g PCE/binder (= 1 wt. % superplasticizer) was measured as 7 ± 0.2 and 3.1 ± 0.3 mg/g after 15 and 60 min hydration, respectively. These amounts indicate that more than 30 % of initial copolymer still remains in the pore solution after 60 min. The XRD analysis of neat calcined clay particles (Figure 4.8a) demonstrates an interlayer spacing (d-spacing) of 0.75 nm, which is in good agreement with reported values in literature [42]. When mixed with synthetic pore solution containing AMPS-PCE2, similar d-spacing was recorded confirming that copolymer molecules interact only with the surface of clay particles and no intercalation occurs during the adsorption process. Size distribution of AMPS-PCE2 in extracted pore solution of L15 with and without addition of 0.2 mol/l Na_2SO_4 (Figure 4.8b) shows that increase in the concentration of sulfate ions induces no change in the steric size of the copolymer. Therefore, it can be inferred that high initial workability and fluidity retention of blends are due to gradual adsorption of AMPS-PCEs to the surface of particles (Figure 4.4b and 4.5) and stability of steric size of the superplasticizer (Figure 4.8b).

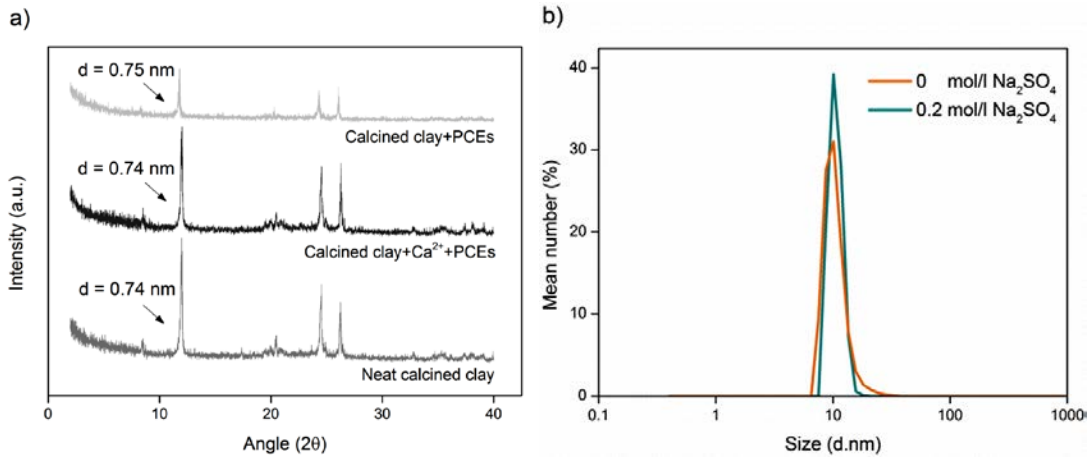

Figure 4.8 a) XRD of calcined clay particles in the presence and absence of AMPS-PCE2 and b) size distributionof polymer coils in pore solution of L15 with Na2SO4

4.6 Mechanical strength and pozzolanic reactions

Figure 4.9 demonstrates compressive strength of hydrated blends at different ages. All mixtures displayed lower strength compared to reference OPC sample. The G1.5 sample exhibited the highest strength among the blends at 1-day and 28-day that are 67% and 75% of the OPC strength, respectively. It is worth mentioning that no real gypsum adjustment was applied according to the cement composition.

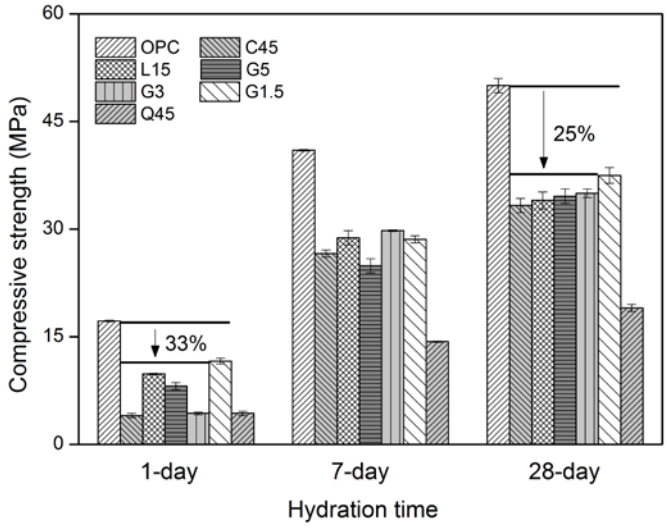

Figure 4.9 Compressive strength of blends at different ages

The evolution of calcium hydroxide (CH) of blends and reference samples was shown in Figure 4.10. The tangent method was used to quantify CH content from the weight loss between 450 and 600 °C and expressed per unit weight of cement [43].

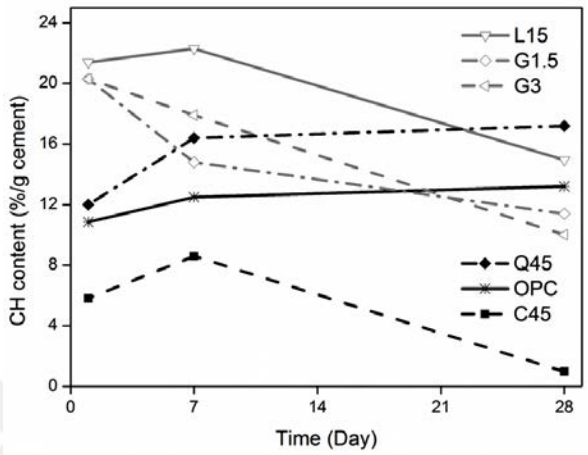

Figure 4.10 Variation of the CH content in the pastes with hydration time

Sample with 45 % quartz substitution (Q45) expectedly showed a higher CH content compared to OPC at all ages. This behavior can be attributed to the extra space and/or nucleation sites available for the hydrates (filler effect). On the other hand, C45 (45% clay substitution) displayed low CH content in comparison with OPC indicating the significant pozzolanic activity of calcined clay in the blend. In agreement with previous reports on highly substituted OPC-clay blends, this level of calcium hydroxide limit the long term strength development of the blend (Figure 4.9). Therefore, highly substituted OPC blends require extra CH for pozzolanic reaction to form calcium silicate hydrate (C–S–H) [9, 44] and the addition of external lime can compensate the lack of CH. After partial substitution of clay with limestone and gypsum (L15, G1.5, and G3) CH content at 1-day became higher than that of C45. This increase demonstrates that hydration kinetics are dominated by the filler effect [45] since no pozzolanic activity is expected from limestone [9]. At later ages, these samples showed considerable pozzolanic reactions, as indicated by the depletion of the CH content towards 28-day of hydration. According to Antoni et al., the high rate of strength gain in ternary mixtures is due to strong synergistic reaction between calcined clay and limestone to form mono/hemi carboaluminate phases [9]. Notably, the highest rate of strength gain in all samples was observed in G1.5 (Figure 4.9), which coincides with high CH content at 1-day and high rate of CH depletion in time (Figure 4.10).

4.7 Conclusion

A series of PCE-based copolymers composed of AA, AMPS, and PEG was synthesized and their ability to disperse the binder particles (OPC, calcined clay, and limestone), and to provide fluidity retention in the blended cement paste was tested. The modified-PCEs was found to disperse mixtures even at high clay content and high concentration of sulfate ions. Results of XRD and dynamic light scattering revealed that the optimized copolymer does not intercalate into the layered structure of calcined clay and also preserves its steric size in the presence of sulfate ions. This copolymer exhibited controlled adsorption onto the surface of the particles, did not get depleted from the pore solution, and thus, induced fluidity retention for extended amounts of time. We believe the optimization route that we report here will provide insight for the design of other superplasticizers that are compatible with multi-component cement systems.

4.8 Reference

[1] R. Gmür, K.-C. Thienel, N. Beuntner, Influence of aging conditions upon the properties of calcined clay and its performance as supplementary cementitious material, Cement and Concrete Composites, 72 (2016) 114-124.
[2] K.L. Scrivener, A. Nonat, Hydration of cementitious materials, present and future, Cement and Concrete Research, 41 (2011) 651-665.
[3] A. Alujas, R. Fernández, R. Quintana, K.L. Scrivener, F. Martirena, Pozzolanic reactivity of low grade kaolinitic clays: Influence of calcination temperature and impact of calcination products on OPC hydration, Applied Clay Science, 108 (2015) 94-101.
[4] A.A. Ramezanianpour, E. Ghiasvand, I. Nickseresht, M. Mahdikhani, F. Moodi, Influence of various amounts of limestone powder on performance of Portland limestone cement concretes, Cement and Concrete Composites, 31 (2009) 715-720.
[5] M.F. Carrasco, G. Menéndez, V. Bonavetti, E.F. Irassar, Strength optimization of “tailor-made cement” with limestone filler and blast furnace slag, Cement and Concrete Research, 35 (2005) 1324-1331.
[6] M. Moesgaard, D. Herfort, M. Steenberg, L.F. Kirkegaard, Y. Yue, Physical performances of blended cements containing calcium aluminosilicate glass powder and limestone, Cement and Concrete Research, 41 (2011) 359-364.
[7] M. Ghrici, S. Kenai, M. Said-Mansour, Mechanical properties and durability of mortar and concrete containing natural pozzolana and limestone blended cements, Cement and Concrete Composites, 29 (2007) 542-549.
[8] G. Menéndez, V. Bonavetti, E.F. Irassar, Strength development of ternary blended cement with limestone filler and blast-furnace slag, Cement and Concrete Composites, 25 (2003) 61-67.

[9] M. Antoni, J. Rossen, F. Martirena, K. Scrivener, Cement substitution by a combination of metakaolin and limestone, Cement and Concrete Research, 42 (2012) 1579-1589.
[10] F. Avet, R. Snellings, A. Alujas Diaz, M. Ben Haha, K. Scrivener, Development of a new rapid, relevant and reliable (R3) test method to evaluate the pozzolanic reactivity of calcined kaolinitic clays, Cement and Concrete Research, 85 (2016) 1-11.
[11] S. Sánchez Berriel, A. Favier, E. Rosa Domínguez, I.R. Sánchez Machado, U. Heierli, K. Scrivener, F. Martirena Hernández, G. Habert, Assessing the environmental and economic potential of Limestone Calcined Clay Cement in Cuba, Journal of Cleaner Production, 124 (2016) 361-369.
[12] L. Zhang, Q. Lu, Z. Xu, Q. Liu, H. Zeng, Effect of polycarboxylate ether comb-type polymer on viscosity and interfacial properties of kaolinite clay suspensions, Journal of Colloid and Interface Science, 378 (2012) 222-231.
[13] G. Duan, G. Huang, A. Li, Y. Zhu, Y. Gong, A study of supermolecular polarization of comb-like polycarboxylate admixtures synthesized with polyoxyethylene macromolecules, Journal of Molecular Liquids, 174 (2012) 129-134.
[14] A. Büyükyağcı, G. Tuzcu, L. Aras, Synthesis of copolymers of methoxy polyethylene glycol acrylate and 2-acrylamido-2-methyl-1-propanesulfonic acid: Its characterization and application as superplasticizer in concrete, Cement and Concrete Research, 39 (2009) 629-635.
[15] A. Habbaba, A. Lange, J. Plank, Synthesis and performance of a modified polycarboxylate dispersant for concrete possessing enhanced cement compatibility, Journal of Applied Polymer Science, 129 (2013) 346-353.
[16] W. Fan, F. Stoffelbach, J. Rieger, L. Regnaud, A. Vichot, B. Bresson, N. Lequeux, A new class of organosilane-modified polycarboxylate superplasticizers with low sulfate sensitivity, Cement and Concrete Research, 42 (2012) 166-172.
[17] L. Lei, J. Plank, A concept for a polycarboxylate superplasticizer possessing enhanced clay tolerance, Cement and Concrete Research, 42 (2012) 1299-1306.
[18] O. Akhlaghi, O. Akbulut, Y.Z. Menceloglu, Extensional rheology and stability behavior of alumina suspensions in the presence of AMPS-modified polycarboxylate ether-based copolymers, Colloid and Polymer Science, 293 (2015) 2867-2876.
[19] T.-S. Liao, C.-L. Hwang, Y.-S. Ye, K.-C. Hsu, Effects of a carboxylic acid/sulfonic acid copolymer on the material properties of cementitious materials, Cement and Concrete Research, 36 (2006) 650-655.
[20] R.I. Masel, Principles of adsorption and reaction on solid surfaces, John Wiley & Sons, 1996.
[21] M.d.M. Alonso, M. Palacios, F. Puertas, Effect of Polycarboxylate–Ether Admixtures on Calcium Aluminate Cement Pastes. Part 1: Compatibility Studies, Industrial & Engineering Chemistry Research, 52 (2013) 17323-17329.
[22] H.B. Bey, J. Hot, R. Baumann, N. Roussel, Consequences of competitive adsorption between polymers on the rheological behaviour of cement pastes, Cement and Concrete Composites, 54 (2014) 17-20.
[23] K. Yoshioka, E.-i. Tazawa, K. Kawai, T. Enohata, Adsorption characteristics of superplasticizers on cement component minerals, Cement and Concrete Research, 32 (2002) 1507-1513.
[24] A. Zingg, F. Winnefeld, L. Holzer, J. Pakusch, S. Becker, L. Gauckler, Adsorption of polyelectrolytes and its influence on the rheology, zeta potential, and microstructure of

various cement and hydrate phases, Journal of Colloid and Interface Science, 323 (2008) 301-312.
[25] I. Navarro-Blasco, M. Pérez-Nicolás, J.M. Fernández, A. Duran, R. Sirera, J.I. Alvarez, Assessment of the interaction of polycarboxylate superplasticizers in hydrated lime pastes modified with nanosilica or metakaolin as pozzolanic reactives, Construction and Building Materials, 73 (2014) 1-12.
[26] N. Mikanovic, C. Jolicoeur, Influence of superplasticizers on the rheology and stability of limestone and cement pastes, Cement and Concrete Research, 38 (2008) 907-919.
[27] Y. Zhang, X. Kong, Correlations of the dispersing capability of NSF and PCE types of superplasticizer and their impacts on cement hydration with the adsorption in fresh cement pastes, Cement and Concrete Research, 69 (2015) 1-9.
[28] T. Sowoidnich, T. Rachowski, C. Rößler, A. Völkel, H.-M. Ludwig, Calcium complexation and cluster formation as principal modes of action of polymers used as superplasticizer in cement systems, Cement and Concrete Research, 73 (2015) 42-50.
[29] J. Plank, M. Gretz, Study on the interaction between anionic and cationic latex particles and Portland cement, Colloids and Surfaces A: Physicochemical and Engineering Aspects, 330 (2008) 227-233.
[30] Y.-R. Zhang, X.-M. Kong, Z.-B. Lu, Z.-C. Lu, S.-S. Hou, Effects of the charge characteristics of polycarboxylate superplasticizers on the adsorption and the retardation in cement pastes, Cement and Concrete Research, 67 (2015) 184-196.
[31] B.L. Rivas, E. Pereira, A. Maureira, Functional water-soluble polymers: polymer–metal ion removal and biocide properties, Polymer International, 58 (2009) 1093-1114.
[32] K. Naka, Biomineralization II Mineralization Using Synthetic Polymers and Templates, Springer, 2007.
[33] A. Yahia, M. Tanimura, Y. Shimoyama, Rheological properties of highly flowable mortar containing limestone filler-effect of powder content and W/C ratio, Cement and Concrete Research, 35 (2005) 532-539.
[34] P.S. Bhosale, J.C. Berg, Poly(acrylic acid) as a rheology modifier for dense alumina dispersions in high ionic strength environments, Colloids and Surfaces A: Physicochemical and Engineering Aspects, 362 (2010) 71-76.
[35] T. Okamura, H. Harada, M. Daimon, Influence of calcium sulfate in belite-rich cement on the change in fluidity of mortar with time, Cement and Concrete Research, 28 (1998) 1297-1308.
[36] J. Cheung, A. Jeknavorian, L. Roberts, D. Silva, Impact of admixtures on the hydration kinetics of Portland cement, Cement and Concrete Research, 41 (2011) 1289-1309.
[37] G. Sua-iam, P. Sokrai, N. Makul, Novel ternary blends of Type 1 Portland cement, residual rice husk ash, and limestone powder to improve the properties of self-compacting concrete, Construction and Building Materials, 125 (2016) 1028-1034.
[38] B. Felekoğlu, H. Sarıkahya, Effect of chemical structure of polycarboxylate-based superplasticizers on workability retention of self-compacting concrete, Construction and Building Materials, 22 (2008) 1972-1980.
[39] T.M. Vickers Jr, S.A. Farrington, J.R. Bury, L.E. Brower, Influence of dispersant structure and mixing speed on concrete slump retention, Cement and Concrete Research, 35 (2005) 1882-1890.

[40] O. Akhlaghi, Y.Z. Menceloglu, O. Akbulut, Poly(carboxylate ether)-based superplasticizer achieves workability retention in calcium aluminate cement, Scientific Reports, 7 (2017) 41743.
[41] K. Yamada, S. Ogawa, S. Hanehara, Controlling of the adsorption and dispersing force of polycarboxylate-type superplasticizer by sulfate ion concentration in aqueous phase, Cement and Concrete Research, 31 (2001) 375-383.
[42] L. Lei, J. Plank, A study on the impact of different clay minerals on the dispersing force of conventional and modified vinyl ether based polycarboxylate superplasticizers, Cement and Concrete Research, 60 (2014) 1-10.
[43] B.K. Marsh, R.L. Day, Pozzolanic and cementitious reactions of fly ash in blended cement pastes, Cement and Concrete Research, 18 (1988) 301-310.
[44] P. Shafigh, M.A. Nomeli, U.J. Alengaram, H.B. Mahmud, M.Z. Jumaat, Engineering properties of lightweight aggregate concrete containing limestone powder and high volume fly ash, Journal of Cleaner Production, 135 (2016) 148-157.
[45] B. Lothenbach, K. Scrivener, R.D. Hooton, Supplementary cementitious materials, Cement and Concrete Research, 41 (2011) 1244-1256.

Chapter 5 Experimental Section

5.1 Materials

An α-Al_2O_3 powder (AKP-500, Sumitomo Chemical Company) was used with the mean particle size of 220 nm and specific surface area of 17 m^2/g determined by BET method. Acrylic acid (AA-99%), 2-acrylamido-2-methylpropane sulfonic acid (AMPS, 99%), potassium persulfate (KPS, ≥99.0%), and hydrochloric acid (HCl, 37%) were obtained from Sigma Aldrich. PEG-1000, maleic anhydride (MA, 99%), and sodium hydroxide (NaOH, ≥97%) were purchased from Merck. All reagents were of analytical grade and used as received without further purification.

Ordinary Portland cement (OPC) CEM 1 42.5 R and CAC ISIDAC 40 were provided by, AKCANSA and CIMSA, Turkey, respectively. Physical and chemical properties of cements were listed in Table 5.1.

Table 5.1 Chemical analysis and physical properties of cements

Cement Type		OPC	CAC
Chemical composition (%)	SiO_2	13.37	3.60
	Al_2O_3	4.68	39.80
	Fe_2O_3	3.35	17.05
	CaO	63.08	36.20
	MgO	1.42	0.65
	SO_3	2.71	0.04
	Loss on ignition	3.30	0.30
Physical properties	Density (g/cm^3)	3.15	3.25
	Fineness (Blaine) (cm^2/g)	3275	3000
	BET surface area (m^2/g)	1.65	2.2
	Initial setting time	155	280
	Final setting time	250	295
	Residue in 45 μm sieve (%)	0	23
	Residue in 90 μm sieve (%)	0.3	6.5
Mechanical properties		2-day: 24.0 (MPa) 28-day: 52.6 (MPa)	6 Hours: 47 (MPa) 24 Hours: 70 (MPa)

Calcium carbonate ($CaCO_3$) was purchased from Sigma-Aldrich. The clay was calcined at 800 °C in a semi-industrial rotary kiln with a residence time of 15 min. The Rietveld analysis on calcined clay showed that it contains 42 % calcined kaolinite (metakaolin) and the rest is uncalcined kaolinite, quartz, and traces of illite, anatase, and hematite. Chemical and physical properties of $CaCO_3$ were listed in Table 5.2. Raw clay contained 42 % kaolinite and the specific surface area of calcined particles was measured as 10.5 m^2/g by N_2 adsorption method.

Table 5.2 Physical and chemical properties of $CaCO_3$

Density (g/cm^3)	2.93
BET surface area (m^2/g)	8.2
Sulfate (SO_4^{2-})	≤0.01%
Chloride	≤0.001%
Fluoride	≤0.0015%
K	≤0.01%
Na	≤0.1%
Impurities	≤0.03%

5.2 Synthesis and characterization of copolymers

5.2.1 Synthesis of copolymers

Equimolar amounts of PEG-1000 and maleic anhydride were charged in a 250 ml three neck flask and the reaction was heated up to 90 °C. The reaction medium was kept under nitrogen for 2 hours; then, cooled to room temperature. We used this product reffered to as PEGMA for polymerization without any purification.

In a typical aqueous free radical polymerization, we first prepared 15 wt% aqueous solutions of reactants with different molar ratios in 110 ml deionized water. Subsequently, pH of the mixture was adjusted by using aqueous solutions of 0.1M NaOH and HCl. Then, this mixture was charged into a three neck flask connected to a reflux condenser and nitrogen was purged for 30 min to remove free oxygen. After 30 min, the flask was heated up to 50 °C and 10 ml aqueous solution of 0.25 g KPS, the initiator, was added to the reaction chamber. After 50 min, we raised temperature to 60 °C and added the 10 ml solution of 0.25 g KPS to the medium for the second time and kept it at this temperature for 75 min. We, then, increased the temperature to 80 °C and the reaction continued for another 4 hours. Finally, the reaction medium was cool down to room temperature, copolymers were precipitated in ethanol, and the product was dried under vacuum at 60 °C until reaching a constant weight.

5.2.2 Characterization of copolymers

Chemical and structural characterization of copolymers was carried out by nuclear magnetic resonance (NMR, Varian Unity Inova 500MHz spectrometer) and dilute solution viscometry (0.2 – 0.5 g/dl, Cannon glass capillary viscometer 1C) at room temperature (22 °C), respectively. Intrinsic viscosities were obtained through extrapolation of reduced viscosities to zero concentration of copolymers. We repeated each test for 3 times and reported the average value.

Density if anionic sites and Ca-complexation ability of copolymers were determined by titration method with a HI-2211 bench top pH meter on 50 ml solution of 1 mg/ml copolymer/water at 22 ± 2 °C. Copolymer solutions were titrated with a 0.1 M NaOH and 0.02 M $Ca(OH)_2$.

Copolymers were characterized by gel permeation chromatography (GPC, Agilent 1260 Infinity equipped with refractive index detector) in aqueous solution of 0.14 mol/l NaCl, 0.01 mol/l Na_2HPO_4 and 0.01 mol/l $NaNO_3$ at a flow rate of 0.7 ml/min.

5.3 Preparation and characterization of alumina samples

5.3.1 Sample preparation

Alumina suspensions were prepared by adding 0.01 wt% alumina particles to a solution containing different amount of copolymers and, then, using ultrasound probe (Vibra Cell 75041, Bioblock Scientific) for 5 min in pulse mode to break soft agglomerations. To monitor the effect of time on particle size of suspensions, all specimens remained uninterrupted throughout the testing. Each test was repeated 6 times with 20 cycles and average value was reported.

5.3.2 Stability and gravity-settling

Stability of alumina suspensions was determined by measuring particle size distribution and hydrodynamic radius (r_h) of alumina suspensions with and without copolymers (Zetasizer nanoseries, Malvern Instruments, Ltd.).

To observe the effect of different copolymers on stability of alumina suspensions, a gravity-settling based test was designed. Suspensions with 4 wt% alumina particles and 2

wt% copolymers (compared to alumina particles) were prepared in native pH of suspensions and then placed in 100 ml graduated cylinder. We took 1 ml of samples at the depth of 60 ml by using a stainless steel needle connected to a 10 ml syringe. These samples were immediately placed in a moisture analyzer (Shimadzu uniBloc MOC63u) to measure the solid content.

5.3.3 Electro-kinetic study

A zeta potential analyzer (Zetasizer nanoseries, Malvern Instruments) was used to monitor the electrokinetic behavior of alumina particles in the presence of different amounts of copolymers. After addition 0.001 wt% alumina particles to polymer solutions and 1 hour stirring, pH of the mixture was adjusted to 2–12. Subsequently, 6 measurements with at least 20 cycles were performed at 25 °C and the average value was reported.

5.3.4 Isothermal adsorption

Adsorption behavior of copolymers was investigated by using UV-vis spectroscopy (UV-3150 Shimadzu spectrometer) and thermogravimetrical analysis (Netzsch STA 449C Jupiter thermal analyzer). Alumina suspensions with 4 wt% of particles and different amounts of copolymers were prepared. After 3 hours of stirring, suspensions were centrifuged to separate the alumina particles. The amount of adsorbed polymer was quantified by measuring the difference between UV-adsorption of supernatant and bulk concentration of copolymers before addition of alumina particles. Moreover, the separated particles were used for thermogravimetrical analysis (TGA, Netzsch STA 449C Jupiter thermal analyzer). To eliminate unadsorbed and weakly bonded copolymers, the separated particles were redispersed in water and then centrifuged at 4,500 rcf for 1 hour. This process was repeated for six times following by drying at 70 °C under moderate vacuum for 3 days. Thereafter, TGA was carried out by heating up the dried samples at 10 K/min from room temperature to 600 °C under nitrogen atmosphere.

5.3.5 Rheological study

The rotational rheological measurements were conducted in Anton-Paar MCR 302 rheometer with cone-plate geometry of 50 mm/2° and a gap size of 0.208 mm. After loading of each sample, a thin layer of low-viscosity paraffin oil was employed around the

outer edge of the plates to protect the sample from evaporation. Temperature was set to 25 °C and the shear rate was changed from 0.1 to 1000 s^{-1}.

The extensional rheological measurements were carried out by using a capillary breakup extensional rheometer (HAAKE CaBER 1, Thermo Scientific, Germany) with two plates which have a diameter of 6 mm. Plate separation was changed from L_0 = 2 mm to L_f = 7.6 mm within 50 ms. The extension rate ($\dot{\varepsilon}$), 26.7 s^{-1}, was set according to the relation $L_f = L_0 \exp(\dot{\varepsilon}t)$, where t is time (s). After establishing liquid bridge, the midpoint diameter (D(t)) was monitored as a function of time using the laser micrometer. Suspensions with 20–45 vol% alumina particles and different amounts of copolymers were prepared by using ultrasound probe in pulse mode and stirring for 24 hours in a capped container to prevent evaporation. All samples were tested at ambient temperature immediately after stopping the stirring process.

5.3.6 Machining

For machining, the green bodies were drilled 5 mm deep with 1.1 mm to 8.2 mm drill bits using conventional mounting heads. Machining speeds were 700–1200 rpm for lathing and 500–900 rpm for drilling. Drilling deeper than 4–5 mm without getting rid of excess swarf initiated internal cracks. Machined samples were sintered at 1500°C for 2 hours with a heating rate of 5°C/min with no binder burnout step. Shrinkage rates were reported based on measurements from 25 samples.

5.3.7 Mechanical properties

Compression tests on green bodies were performed with Zwick/Roell Z100 universal testing machine according to ASTM 773 standard. All suspensions were cast in homemade gypsum molds (3/4 vol/vol gypsum to water ratio) with an inner diameter of 11 mm and a height of 15 mm. All samples were de-molded after 24 hours and then dried at 70°C for 24 hours. Each experiment was repeated 5 times.

5.3.8 Density measurement

AccupycII-1340 gas pycnometer was used to measure percentage of theoretical density of alumina green bodies. Before measurement, each sample was covered with silicone oil to prevent penetration of helium through open pores.

5.4 Sample proportioning and characterization of cementitious suspensions

5.4.1 Sample preparation

Binders with different amounts of calcined clay, limestone, and gypsum were first dry-mixed with OPC for 5 min. Certain amounts of these blends were then charged to 100 ml of polymer solutions containing 0–15 mg/g superplasticizer/binder (0–1.5 wt. %) to cast pastes with water to binder ratio (w/b) of 0.4. All binders were first hand-mixed for 30 sec and then stirred by Heidolph RZR 2102 mixer equipped with a 4-blade stainless steel propeller for 5 min at 1000 rpm. Such a high-shear mixing regime was used to ensure good dispersion of particles and homogeneous pastes.

5.4.2 Rheologial study

Rheological behavior of cement pastes was characterized by determining the plastic viscosity and yield stress using Anton-Paar MCR 302 rheometer equipped with cone-plate geometry of 50 mm/2° and a gap size of 0.208 mm at 25 ± 0.1 °C. All cement pastes were loaded immediately after cessation of the mixing process. After loading each sample, a thin layer of low viscosity paraffin oil (~150 mPa.s at 20 °C) was employed around the outer edge of the plates to protect the sample from evaporation. Rheological measurements were carried out by the measurement sequence as following; cement pastes were first kept under constant shear rate of 100 s^{-1} for 60 sec to ensure the structural breakdown. An increasing shear rate ramp from 10 to 100 s^{-1} in 150 sec was then applied followed by a decreasing ramp rate from 100 s^{-1} to 10 s^{-1} in 150 sec. The flow curve of descending shear rates was modeled using Bingham equation ($\tau = \tau_0 + \eta\dot{\gamma}$) where τ is the shear stress (Pa), τ_0 is the yield stress (Y-intercept, Pa), and η is plastic viscosity (Pa.s). When pastes are totally deflocculated, demonstrated by no hysteresis cycle, they behaved like Bingham fluids and the shear rate descent curves could be fitted to the Bingham equation. In some cases, the relationship between shear rate and shear stress was not linear. Therefore, plastic viscosity

and shear yield stress were assessed from the relationship between shear stress and shear rate such that shear yield stress and plastic viscosity were defined as the intercept point of the linear part nearest the Y-axis and the slope of the linear part of the relationship around 50 to 100 s^{-1}, respectively.

5.4.3 Workability

Mini slump test was carried out at 22 ± 2 °C according to ASTM C143. In this test, a cone with bottom diameter, top diameter, and height of 40 mm, 20 mm, and 60 mm, respectively, is filled with the paste and spread diameter is recorded after pulling out the cone. Average value of two crossing spread diameters after 2 times repetition of each test was reported as the test result. Time dependent workability tests (slump retention) were performed at the intervals of 15, 30, 45, and 60 min after the first touch of water. Four different batches were prepared and sealed to prevent the evaporation of water. The pastes, were, then stirred at 300 rpm for 30 sec and slump tests were conducted after 15 sec of resting time of the pastes in the slump cone.

5.4.4 Isothermal adsorption

Adsorption of AMPS-PCEs on different components was evaluated using depletion method in synthetic pore solution prepared from 0.6 g/L $CaSO_4 \cdot 2H_2O$, 5.2 g/L NaOH, 17.9 g/L KOH, and 2.4 g/L $Ca(OH)_2$ in 1 L of deionized water (pH of ~ 13.5)[1]. Suspensions of OPC, clay, and limestone with 0–10 mg/g AMPS-PCEs/particle at a pore solution to particle ratio of 2 were prepared. After 15 min of stirring, the suspensions were centrifuged at 10,000 rpm for 10 min to separate the particles. The liquid phase was diluted by 1/2 (vol/vol) with 1.5 M HCl and filtrated through a 0.2 μm filter to remove any contaminants. The amount of adsorbed polymer was quantified by measuring the difference between intensity value of the scattered light (Zetasizer ZS, Malvern Instruments) of supernatant and bulk concentration of the polymer before addition of particles. Test result is the average of three independent measurements with at least 15 runs.

5.4.5 Electro-kinetic study

A zeta potential analyzer (Zetasizer ZS, Malvern Instruments) was used to monitor the electro-kinetic behavior of particles in synthetic pore solution and water at different

amounts of superplasticizers. The suspensions with solution to binder ratio of 40 and AMPS-PCEs/particle of 0–10 mg/g were mixed by a magnetic stirrer for 10 min, dispersed by a bath sonicator for 3 min and again, magnetically stirred for another 2 min. Prior to the measurement, suspensions were diluted by deionized water (1/5 vol/vol) to adjust the conductivity of the medium to ~ 18 mS/cm. Each result represents the average value of 6 measurements, with 15 to 20 runs per measurement.

5.4.6 Stability

Dispersing state of cement particles in aqueous medium was determined by dynamic light scattering (DLS) and measuring the Z-average (average particle size) of cement suspensions with and without polymers (Zetasizer nanoseries, Malvern Instruments, Ltd.). The suspensions with w/c of 40 and PCEs/cement of 0–10 mg/g were mixed by a magnetic stirrer for 10 min and then diluted by distilled water with a ratio of 1 to 20 (v/v). Each result represents the average value of 6 measurements, with 15 to 20 runs for each measurement.

5.4.7 Structural study

To investigate the possible intercalation of AMPS-PCEs molecules into clay structure, X-ray diffraction (XRD) was carried out via BrukerAXS diffractometer fitted with a Siemens X-ray gun with 0.154 nm Cu Kα radiation. XRD was performed at room temperature with the scan range of 2θ =2–40°, step size of 1 s/step, step width of 0.01° 2θ/step, and spin revolution time of 4 s. All samples were prepared by mixing of 2 g of calcined clay sample and 80 g of water with or without 0.02 g AMPS-PCEs and 0.088 g $CaCl_2$ (0.4 g/l Ca^{2+} as the synthetic pore solution for 15 min followed by centrifugation at 5,000 rpm for 10 min. The solid residues were vacuum-dried for 12 hours at 80 °C and grounded before measurement.

5.4.8 Mechanical properties

Plastic molds with a diameter of 26.2 ± 0.3 mm and a height of 53 ± 1 mm were used to obtain cylindrical specimens for compression tests. After casting the pastes, all containers were sealed for 24 hours followed by demolding and placing into water at 22 ± 2

°C for up to 28 days. Compressive strength of specimens at different ages was examined by Zwick/Roell Z100 testing machine according to EN-196 standard.

5.4.9 Thermo-gravimetric analysis

After compression tests, the specimens were crushed and put in isopropanol for 5–7 days to stop hydration, then vacuum dried at 40 °C for 3 days and preserved in a sealed container for thermo-gravimetric analysis (TGA, Netzsch STA 449C). To determine the amount of calcium hydroxide (CH) in hydrated samples, TGA was performed on ~ 50 mg specimens using a heating rate of 10 K/min under nitrogen in the temperature range of 30–1000 °C.

5.4.10 Isothermal calorimetry

A TAM Air isothermal calorimeter from Thermometric was used. It consists of 8 parallel twin type measurement channels. One cell is dedicated to the sample, the other to a reference vessel. The reference vessel containing 10 g of deionized water was used to reduce the signal to noise ratio and to correct measurement and temperature artifacts. 20 ml glass ampoules were used for both the sample and the reference container. Each channel is independent from the other channels and was calibrated before starting experiments. The baseline was recorded for approximately 30 minutes before ampoules placement inside the calorimeter and 30 min after removing of the ampoules. The procedure for mixing was 2 minutes of mechanical mixing followed by the immediate placement of the ampoules inside the calorimeter, to monitor the hydration from the earliest time possible. All systems were mixed at a water to cement ratio (w/c) of 0.4 with deionized water. The mass of paste was ~ 10 g.

5.4.11 Conductivity

Conductivity measurements were carried out with Zetasizer nanoseries (Malvern Instruments). PCEs solutions (1 mg/ml PCEs/water) were prepared and titrated with a 0.02 M $Ca(OH)_2$.

5.4.12 Specific surface area

The Brunauer-Emmett-Teller (BET) specific surface area of samples was determined by analyzing the standard nitrogen adsorption isotherms at 77 K using nova 2200e, Quantachrome instruments. Suspensions with w/c of 0.4 (OPC) and 0.3 (CAC) were mixed for 1–5 min followed by centrifugation at 5000 rpm for 5 min. OPC and CAC particles were then redispersed in 2-propanol and acetone, respectively and centrifuged at 5000 rpm for 15 min. This process was repeated for 3 times following by vacuum drying at 40 °C for 3 days.